New Journal of Physics
The open-access journal for physics

Optical study of orbital excitations in transition-metal oxides

R Rückamp[1], E Benckiser[1], M W Haverkort[1], H Roth[1], T Lorenz[1], A Freimuth[1], L Jongen[2], A Möller[2], G Meyer[2], P Reutler[3], B Büchner[4], A Revcolevschi[3], S-W Cheong[5], C Sekar[4], G Krabbes[4] and M Grüninger[1,6,7]

[1] II. Physikalisches Institut, Universität zu Köln, Zülpicher Str. 77, D-50937 Köln, Germany
[2] Institut für Anorganische Chemie, Universität zu Köln, D-50937 Köln, Germany
[3] Laboratoire de Chimie des Solides, Université Paris-Sud, 91405 Orsay Cédex, France
[4] IFW Dresden, D-01171 Dresden, Germany
[5] Department of Physics and Astronomy, Rutgers University, Piscataway, NJ 08854, USA
[6] II. Physikalisches Institut, RWTH Aachen, D-52056 Aachen, Germany
E-mail: grueninger@physik.rwth-aachen.de

New Journal of Physics **7** (2005) 144
Received 7 February 2005
Published 17 June 2005
Online at http://www.njp.org/
doi:10.1088/1367-2630/7/1/144

Abstract. The orbital excitations of a series of transition-metal compounds are studied by means of optical spectroscopy. Our aim was to identify signatures of collective orbital excitations by comparison with experimental and theoretical results for predominantly local crystal-field excitations. To this end, we have studied TiOCl, $RTiO_3$ (R = La, Sm and Y), $LaMnO_3$, Y_2BaNiO_5, $CaCu_2O_3$ and $K_4Cu_4OCl_{10}$, ranging from early to late transition-metal ions, from t_{2g} to e_g systems, and including systems in which the exchange coupling is predominantly three-dimensional, one-dimensional or zero-dimensional. With the exception of $LaMnO_3$, we find orbital excitations in all compounds. We discuss the competition between orbital fluctuations (for dominant exchange coupling) and crystal-field splitting (for dominant coupling to the lattice). Comparison of our experimental results with configuration-interaction cluster calculations in general yields good agreement, demonstrating that the coupling to the lattice is important for a

[7] Author to whom any correspondence should be addressed.

PII: S1367-2630(05)94444-3

quantitative description of the orbital excitations in these compounds. However, detailed theoretical predictions for the contribution of collective orbital modes to the optical conductivity (e.g. the line shape or the polarization dependence) are required to decide on a possible contribution of orbital fluctuations at low energies, in particular, in case of the orbital excitations at $\approx$0.25 eV in $RTiO_3$. Further calculations are called for which take into account the exchange interactions between the orbitals and the coupling to the lattice on an equal footing.

Contents

1. Introduction

The large variety of interesting physical phenomena observed in transition-metal oxides results from the strong electronic correlations within the partly filled 3d shell [1]. The correlated 3d electrons carry charge, spin and orbital degrees of freedom, and often they are strongly coupled to the lattice. Due to the complex interplay of these degrees of freedom [2], a subtle change of a single parameter such as the bond angle or the temperature may result in a dramatic change of the physical properties. A prerequisite for a quantitative description of this complex interplay is a detailed understanding of the physics of each degree of freedom separately. Over the last few years, a lot of progress was achieved regarding the properties of, e.g., low-dimensional quantum spin systems [3, 4], in which the charge degrees of freedom are frozen out due to the formation of a Mott–Hubbard insulator at half filling. Many fascinating phenomena have been discovered such as the absence of long-range order even at zero temperature in one-dimensional spin liquids [5, 6], the opening up of spin gaps in even-leg $S = 1/2$ ladders [7] or in the $S = 1$ Haldane chain [8], and novel excitations such as spinons [9]–[12], triplons [13] or two-triplon bound states [14, 15]. The coupling of spin and charge degrees of freedom may give rise to superconductivity in doped spin ladders [16]–[18] and is one of the key features in the field of high-temperature

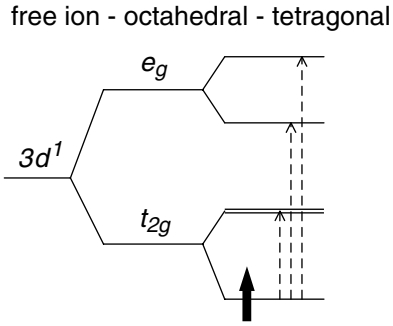

Figure 1. Crystal-field splitting of the 3d states in an octahedral environment (e_g, t_{2g}) and in the case of tetragonal symmetry. For a $3d^1$ ion in tetragonal symmetry, one expects three distinct d–d transitions.

superconductivity in the cuprates. The interplay of the spins and the lattice has been analysed in great detail in the spin-Peierls system $CuGeO_3$.

Orbital and spin degrees of freedom are intimately connected with each other, and it is tempting to speculate about novel quantum phenomena related to the orbital degrees of freedom. Some interesting examples which have been discussed recently are orbital liquids [19]–[22], strong orbital fluctuations, an orbital Peierls state [23]–[25] and orbital waves (orbitons) [26]–[30]. Candidates for the realization of these phenomena are $LaTiO_3$ [21, 31], TiOCl [32, 33], YVO_3 [34] and $LaMnO_3$ [26], respectively. However, many of these claims are heavily debated in the literature [35]–[53]. These novel phenomena are based on the exchange interactions between orbitals on adjacent sites. A crucial assumption is that some orbitals are (nearly) degenerate. For instance, the discussion of an orbital liquid in pseudo-cubic titanate perovskites [21] starts from a partially filled t_{2g} level and assumes that the degeneracy is lifted by quantum fluctuations based on exchange interactions. However, the orbital degeneracy may also be lifted by the coupling to the lattice (Jahn–Teller effect). Drawing an analogy with the spin degrees of freedom, the situation is similar to the case of two antiferromagnetically coupled spins in an external magnetic field. If the exchange interactions dominate, the two spins will form a singlet. However, if the external magnetic field dominates, the spins will align parallel to the field, and the spin fluctuations are strongly suppressed. For the orbital degrees of freedom, we are thus confronted with two central questions: which of the two mechanisms yields the larger energy gain? How strongly are the orbital fluctuations quenched by the coupling to the lattice? For experimental studies, the challenge clearly is to find a compound in which the exchange interactions between the orbitals are significant, while the coupling to the lattice and the corresponding crystal-field splitting are relatively small. Pseudo-cubic $3d^1$ or $3d^2$ perovskites are promising candidates, since orbital quantum fluctuations are particularly large for t_{2g} electrons (threefold degeneracy) in a cubic lattice (large frustration of the orbital interactions) [21], while the coupling to the lattice is smaller for t_{2g} electrons than for e_g electrons in octahedral symmetry.

Studies of the coupling of orbital degrees of freedom to the lattice have a long history in the context of crystal-field transitions [54]. In a crystalline environment, the fivefold degeneracy of the 3d orbitals is (partially) lifted by the electrostatic crystal field and by hybridization with the ligand ions. For instance, in local cubic symmetry, one finds a splitting into a triply degenerate t_{2g} level and a doubly degenerate e_g level (see figure 1). The value of this splitting is denoted by

10 Dq. For simplicity, we consider an insulating host lattice plus a Ti^{3+} impurity with a single electron in the 3d shell. In the ground state, this electron occupies the energetically lowest crystal-field level. An orbital or crystal-field excitation corresponds to the excitation of this electron into a higher-lying orbital, e.g. from the t_{2g} level into the e_g level (see figure 1). For the example of $3d^1$ Ti^{3+}, the excitation energy of this process typically amounts to $10\,Dq \gtrsim 2$ eV [55]. Similar values of 10 Dq are also found for other transition-metal ions. This value is lying in the visible range and explains the vivid colours of gemstones such as ruby (impurities of Cr_2O_3 in an Al_2O_3 host lattice). Coming back to the analogy with the spin degrees of freedom, such a crystal-field excitation is similar to flipping an impurity spin in a tremendous external magnetic field. The challenge is to reduce the 'external' field and to enter the realm where the collective nature of the excitations becomes relevant.

In a nearly cubic environment, the splitting of the t_{2g} subshell is much smaller than 10 Dq. In the case of Ti^{3+} impurities in an Al_2O_3 host lattice, absorption features have been observed at about 5 and 13 meV in infrared transmittance measurements [56]. The splitting was attributed to the low-symmetry crystal field and spin–orbit coupling. However, the level splitting of 13 meV is much smaller than predicted by crystal-field theory, which was tentatively attributed to a reduction of the crystal field by a dynamic Jahn–Teller effect [56].

Intersite interactions between orbitals may already be important in the case of impurities embedded into a host lattice (if the impurity concentration is large enough). Back in 1959, it was realized that the interactions between Cr^{3+} ions in concentrated ruby give rise to a new structure in the optical data [57]. If the transition-metal ions form a lattice, the interactions between neighbouring sites give rise to a finite hopping probability of an excited state from one site to another. Thus the excitation gains a finite dispersion or band width. It can be described in terms of a Frenkel exciton, i.e. a tightly bound electron–hole pair. The electron and the hole occupy the same site, but the pair may hop from one ion to another. In a translationally invariant system, the exciton is described by a superposition of local crystal-field excitations with a phase factor $\exp(\mathrm{i}kr)$, where k denotes the wave vector and r runs over all transition-metal sites. This does not play a major role in the discussion of crystal-field excitations of 3d electrons in the range of 10 Dq, because the dispersion usually is much smaller than both the excitation energy and the peak width (the latter arises from the coupling to the lattice, see the discussion of the Franck–Condon effect below). However, experimental evidence for a finite dispersion has been derived from the analysis of magnon-sidebands of crystal-field excitations at about 2.3 eV [58].

In a Mott–Hubbard insulator, the energy necessary to create a free electron–hole pair is of the order of U, but the binding energy of a Frenkel exciton is also of the order of U. Thus the Frenkel exciton may exist way below the band gap, and the relevant energy scale is set by the crystal-field splitting and by the hopping amplitude of the exciton between neighbouring sites. Most noteworthy, the band width of a single-doped carrier in an antiferromagnetic Mott insulator is strongly suppressed by the coupling to the spins, so that the band width of an excitonic particle–hole pair may even be larger than the one-particle band width [59].

The novel aspect of orbital waves or orbitons [26]–[30] is that the exchange interactions are assumed to mark the dominant energy scale, minimizing the kinetic energy. In this case, the collective nature of the excitations prevails over the local character, in analogy to spin waves. Note, however, that the orbital degree of freedom does not show continuous rotational symmetry. Orbitons in an orbitally ordered state thus are gapped. The dispersion and the excitation energy may be of comparable magnitude, giving rise to interesting novel effects. Examples are a possible contribution to the specific heat [21, 42], the renormalization of magnon spectra [60] or the

formation of orbiton–magnon bound states [61] due to a coupling between spin and orbital degrees of freedom.

Optical spectroscopy has proven to be an excellent tool for the study of crystal-field excitations [54, 62]. Besides the determination of the excitation energy, it also provides valuable information via an analysis of the line shape observed in the optical conductivity $\sigma(\omega)$. A detailed study of orbital excitations in $\sigma(\omega)$ thus may offer an important test whether novel collective phenomena appear in a particular compound. Here, we present optical data for a series of insulating transition-metal oxides (TiOCl, $RTiO_3$ (R = La, Sm and Y), $LaMnO_3$, Y_2BaNiO_5, $CaCu_2O_3$ and $K_4Cu_4OCl_{10}$)[8], including early and late transition-metal ions, t_{2g} as well as e_g systems, and systems in which the exchange coupling is predominantly three-dimensional, one-dimensional or zero-dimensional. Orbital excitations are observed in the range from about 2.5 eV down to about 0.25 eV. Only in $LaMnO_3$, we did not find any signature of orbital excitations below the band gap. We compare the experimental data with theoretical results for the crystal-field excitations based on the point-charge model and on configuration-interaction (CI) cluster calculations. Our calculations satisfactorily describe all of our optical conductivity data, suggesting that the coupling to the lattice is dominant in these compounds. However, in the case of the low-energy modes ($\approx$0.25 eV) in $RTiO_3$ we cannot exclude a contribution from orbital fluctuations. But our results clearly demonstrate that the coupling to the lattice may not be neglected if one aims at a quantitative description of the orbital excitations of the above compounds. We suspect that this will turn out to be generally valid in insulating compounds. One may hope that the importance of low-energy orbital excitations is enhanced by choosing a system which is closer to a metal–insulator transition.

In the following section, we will discuss the selection rules for the observation of orbital excitations by means of optical spectroscopy. In section 3, the point-charge model and the cluster calculations will be explained, whereas section 4 is devoted to experimental aspects. In sections 5–9, we will present the optical data of TiOCl, $RTiO_3$, $LaMnO_3$, Y_2BaNiO_5, $CaCu_2O_3$ and $K_4Cu_4OCl_{10}$, respectively. Some general conclusions will be given in section 10.

2. Orbital excitations in optical spectroscopy

2.1. The case of a single ion

In the following paragraphs, we first consider the physics of a single ion embedded into a host lattice. The effects of interactions between the transition-metal ions will be addressed in section 2.2.

The dominant contribution to the optical conductivity $\sigma(\omega)$ arises from electric dipole transitions. The matrix element for a d–d transition induced by a photon is proportional to

$$\langle \psi_{final} | \mathbf{p} | \psi_{initial} \rangle .$$

The dipole operator $\mathbf{p}$ has odd parity. Considering a transition-metal site with inversion symmetry, the above matrix element vanishes due to the even parity of the 3d wave functions,

$$\langle \text{even} | \text{odd} | \text{even} \rangle = 0.$$

[8] Parts of the data on $LaMnO_3$ and on $CaCu_2O_3$ have been reported before in [51, 63].

Hence a mere d–d transition is forbidden within the dipole approximation in compounds with inversion symmetry on the transition-metal site, i.e., the d–d transitions do not contribute to $\sigma(\omega)$. However, there are several processes which allow the observation of d–d transitions, but one has to keep in mind that the corresponding features are only weak. In the present paper, we will show examples for orbital excitations observed in $\sigma(\omega)$ which are due to (i) the absence of inversion symmetry on the transition-metal site, (ii) a phonon-activated mechanism and (iii) magnon–exciton sidebands.

A very attractive method for the observation of orbital excitations opens up if the crystal structure does not show inversion symmetry on the transition-metal site, as e.g. in TiOCl (see section 5). In this case, parity is not a good quantum number, so that even and odd states mix. The amount of mixing can be estimated within the point-charge model, see section 3. It depends on the difference in energy between the even (3d) and odd (e.g. 3p or 4p) states and on how strong the deviations from inversion symmetry are. The small spectral weight of the orbital excitations is taken away from the dipole-allowed absorption band, e.g. from the 3d–4p transition. The major advantage of this structurally induced mechanism is that it allows one to make clear predictions on the polarization dependence of the orbital absorption features because the (local) symmetry of the mixed states can be determined unambiguously within the point-charge model. We use the room-temperature structure of TiOCl as an example (see section 5). For this $3d^1$ compound, we found that the lowest valence orbital predominantly shows $d_{y^2-z^2}$ character[9] with a small admixture of p_z character. The first excited state shows pure d_{xy} character, while the second excited state is mixed from d_{yz} and p_y states. Therefore, a dipole transition from the ground state to the second excited state is weakly allowed for light polarization parallel to the y axis, but not for x or z polarization:

$$\langle \alpha' d_{yz} + \beta' p_y | y | \alpha d_{y^2-z^2} + \beta p_z \rangle \neq 0, \tag{1}$$

$$\langle \alpha' d_{yz} + \beta' p_y | x | \alpha d_{y^2-z^2} + \beta p_z \rangle = 0. \tag{2}$$

Such polarization selection rules offer the possibility for a straightforward experimental test.

If the crystal structure shows inversion symmetry on the transition-metal site, this symmetry can be broken by an odd-symmetry phonon which is excited simultaneously with the orbital excitation [54, 62]. This again gives rise to an admixture of a small amount of odd character to the 3d wave function (see figure 2). The dependence on the polarization of the incident light is less pronounced for this phonon-activated mechanism than for the structurally induced mechanism described above, because in general phonons of arbitrary polarization may contribute, i.e. x, y and z character can all be mixed into the 3d states. In order to determine the orbital excitation energy, the phonon energy has to be subtracted from the experimentally observed peak position. One has to keep in mind that different phonons may break the symmetry. Typically, stretching and bending modes of the metal-oxygen bonds are most effective in doing so [54]. These modes have typical energies of the order of 50–80 meV. The fact that phonons with different energies may contribute and that these phonons additionally have some dispersion increases the width of the absorption band (the most important source for the line width is described by the Franck–Condon effect, see below).

[9] The ligands are located approximately along the diagonals of the yz plane, hence $d_{y^2-z^2}$ denotes a state from the t_{2g} subshell.

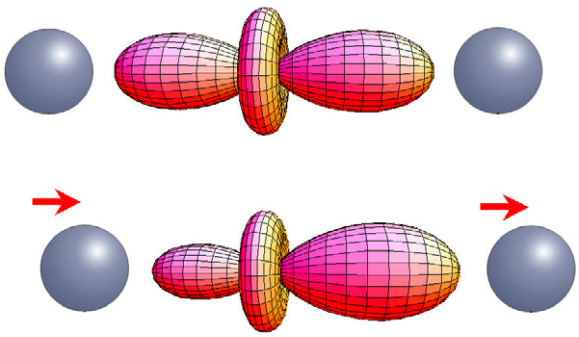

Figure 2. Top: sketch of a $3z^2–r^2$ orbital on a transition-metal site in between two negatively charged ligands. Bottom: exciting a bond-stretching phonon breaks the inversion symmetry on the transition-metal site, thus parity is no longer a good quantum number. This gives rise to a mixing of even and odd states, e.g. of the $3d_{3z^2-r^2}$ state with the $4p_z$ state. The sketch indicates an increased electron density on the right side, where the distance to the negatively charged ligand has increased.

Another way to break the symmetry is to add impurities to the system. However, it has been shown experimentally that this, in general, is by far less effective than the phonon-activated mechanism described above [54]. One way of testing whether a phonon is involved in the infrared absorption process is to compare the energies of the orbital excitations observed in $\sigma(\omega)$ and in Raman scattering. In compounds with inversion symmetry, the exclusion principle states that selection rules for Raman scattering and infrared absorption are mutually exclusive. Orbital excitations can be observed directly in Raman scattering because two photons are involved in the scattering process, thus the odd dipole operator has to be applied twice. The incoming photon excites an electron from a 3d orbital to, e.g., a 4p state, from which it falls back to an excited 3d state under the emission of a photon. Using again the example of a $3d^1$ system, the transition from, e.g., d_{xy} to d_{xz} is Raman active in crossed polarization, for instance for y (z) polarization of the incoming (outgoing) photon:

$$\langle d_{xz}|z|p_x\rangle\langle p_x|y|d_{xy}\rangle \neq 0.$$

Other optical experiments which allow the observation of orbital excitations are, e.g., electroreflectance measurements [64] or third-harmonic spectroscopy [65]. Furthermore, d–d excitations have been studied by means of electron energy loss spectroscopy (EELS) [66].

Thus far we have neglected the spin selection rule. One has to keep in mind that optical spectroscopy with linearly polarized light is only sensitive to spin-conserving excitations, $\Delta S = 0$. This selection rule can be relaxed by taking into account spin–orbit coupling. Another possibility is to excite two spin-carrying modes simultaneously in such a way that the total spin amounts to zero. An orbital excitation from a triplet state to a singlet may gain a finite spectral weight by the simultaneous excitation of a magnon, giving rise to a so-called magnon–exciton sideband [58, 67, 68]. The spectral weight of these processes is even smaller than in the cases discussed above where the spin was not involved. Nevertheless, these processes are dominant in systems with d^5 ions such as Mn^{2+} [58, 68], in which none of the excited states carries the same spin value as the ^6S ground state. In MnF_2, both magnetic-dipole and electric-dipole transitions have been observed [58]. The magnetic-dipole character can be proved experimentally by the

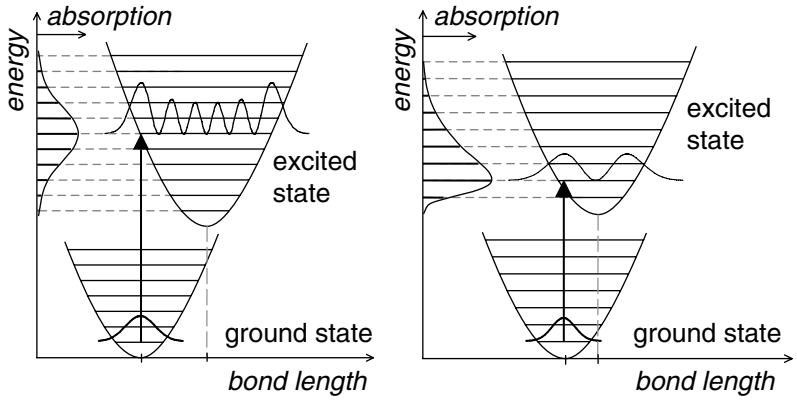

Figure 3. Sketch of the Franck–Condon principle. In both panels, each parabola corresponds to a different orbital state and represents the harmonic potential of the lattice. The lines within a parabola denote phonon excitations. The horizontal position of a parabola indicates the distance to the ligands after the lattice has been allowed to relax in a particular orbital state. Promoting e.g. an electron in an octahedral oxygen cage from $x^2 - y^2$ to $3z^2$ tends to push away the two negatively charged oxygen ligands on the z axis. In general, electronic timescales are much faster than the relaxation time of the lattice. A fast electronic excitation, i.e. without relaxation of the lattice, corresponds to a vertical transition (arrow). The transition probability is proportional to the overlap between the wave functions of the ground state and of the excited state. The thick lines denote the amplitudes of the ground-state wave function and of an excited harmonic oscillator. The strongest overlap is obtained for the level which is closest to where the vertical arrow cuts through a parabola. In the final state, both the lattice and the electronic/orbital subsystem are in an excited state, i.e. the excited states are of mixed character (vibrational + electronic → 'vibronic'). Summing up the contributions from the different excited states results in the broad absorption peak shown on the left in each panel. Due to the dispersion of the phonons and due to the contribution of phonons with different energies, the sharp subbands of individual excited states are usually not resolved in a solid, yielding a single broad band. The width and the line shape of an absorption band in $\sigma(\omega)$ depend on the difference in bond length of the different orbital states. Large differences in the bond length give rise to symmetric absorption bands (left panel), whereas small differences cause a characteristic asymmetric line shape (right panel).

observation of a splitting in an applied magnetic field or by a detailed study of the polarization dependence, i.e., by showing that the absorption features depend on the direction of the magnetic field component and not on the electric field component.

For the discussion of the line shape, one has to take the coupling to the lattice into account. The absorption band will be broadened by phonon sidebands according to the Franck–Condon principle, and the line shape depends on the difference of the relaxed bond lengths of the orbital states involved (for details see the caption of figure 3). We emphasize that this reflects the mixed,

'vibronic' character of the eigenmodes (phonon + orbiton, or vibrational + electronic → 'vibronic' [54]) and thus holds irrespective of the mechanism responsible for the finite spectral weight of an orbital excitation. In particular, these phonon sidebands may not be confused with the phonon-activated mechanism described above and appear also in the case of, e.g., the structurally induced mechanism relevant for TiOCl or in Raman data.

2.2. *Interaction effects*

We have to address the question how to distinguish experimentally between a collective orbital excitation and a predominantly 'local' crystal-field excitation. A direct observation of the dispersion of the orbital-momentum fluctuations by means of inelastic neutron scattering would manifest a watertight proof. While neutron scattering has been used for the study of crystal-field excitations of f-electron compounds [69], we are not aware of such data for the case of 3d electrons. Here, one has to keep in mind that the coupling to the lattice will smear out the orbital excitations significantly. Inelastic x-ray scattering offers another k-dependent tool, but no collective orbital excitations were found in the study of $LaMnO_3$, $KCuF_3$ and $YTiO_3$ presented in this Focus issue [70].

Under the assumption that the dominant energy scale is set by the exchange interactions, the dispersion relations of orbitons have been calculated for the orbitally ordered states of $LaMnO_3$, $LaVO_3$, YVO_3 and $YTiO_3$ [26, 27, 30], and within a model focusing on the orbital fluctuations [28, 29]. Predictions have been derived for inelastic neutron scattering and Raman scattering. In section 2.1 above, we have discussed a Raman process in which the virtual excitation into a p state was assumed to take place on a single site. In case of dominant exchange interactions, a two-site process involving the upper Hubbard band is considered [30], in analogy to the well-known two-magnon Raman scattering. For simplicity, we consider per site one electron and two orbitals. In the first step, the incident photon promotes an electron from site 1 to site 2, which becomes doubly occupied. In the second step, an electron hops back from site 2 to 1 under emission of a photon. In the final state, one or both electrons may be in an excited orbital, i.e., the exchange process may give rise to one-orbiton and/or two-orbiton excitations [30]. Depending on the hopping amplitudes between the different orbitals on adjacent sites, distinct polarization selection rules have been predicted [26, 30].

The excitation of two orbitons with momenta $k_1 = -k_2$, in principle, allows us to probe the orbiton dispersion throughout the entire Brillouin zone, since only the total momentum $k_1 + k_2$ needs to be equal to zero in Raman scattering. Information about the dispersion is contained in the line shape of the two-orbiton Raman band, but a detailed analysis of the line shape encounters several problems: (i) in general, the Raman line shape depends on the frequency of the incident photons (resonance behaviour), (ii) the orbiton–orbiton interactions are essential for the line shape, but have not been taken into account up to now and (iii) the coupling to the lattice reduces the orbiton dispersion.

The optical conductivity thus far has not been considered as a tool for the investigation of orbitons. Starting again from the crystal-field limit, we note that the optical data of a crystal-field Frenkel exciton with a dispersion much smaller than its energy is in principle very similar to the data of a single impurity ion embedded in a host lattice. In particular, optical spectroscopy is restricted to the observation of excitations with momentum $k = 0$, and the selection rules are the same as for the case of a single impurity ion. Nevertheless, the dispersion may play a role if two modes are excited simultaneously, as e.g. in a magnon–exciton sideband [58] or in the

phonon-activated case. Only the total momentum needs to be equal to zero, and one has to sum up contributions from excitons from the entire Brillouin zone.

As far as the intersite exchange processes discussed above for the Raman case are concerned, Khaliullin [71] has pointed out the possibility of two-orbiton-plus-phonon absorption, similar to the two-magnon-plus-phonon absorption proposed by Lorenzana and Sawatzky [72, 73] for spin systems. In systems with inversion symmetry in between adjacent sites, the exchange of two electrons does not give rise to a dipole moment. Similar to the phonon-activated mechanism for the observation of crystal-field transitions described above, this selection rule can be relaxed by the simultaneous excitation of a phonon [72, 73]. The two-magnon-plus-phonon absorption[10] has been established as an interesting tool for studies of antiferromagnetic spin chains, spin ladders and layered antiferromagnets [15, 63], [74]–[78]. Since the phonon contributes to momentum conservation, the optical conductivity probes the two-magnon or two-orbiton spectral function throughout the entire Brillouin zone, in contrast to two-orbiton Raman scattering, which reflects only the $k = 0$ part of the two-orbiton spectrum. Thus, both the line shape and the peak position are expected to be different in $\sigma(\omega)$ as compared to Raman data. In spin systems, the excitation of a single magnon does not contribute to $\sigma(\omega)$ due to the spin selection rule. In the case of orbitons, however, the phonon-activated single-site mechanism used for the study of crystal-field excitations will also be at work if the exchange interactions are dominant. Thus one has to expect a superposition of orbiton-plus-phonon and two-orbiton-plus-phonon contributions.

Thus far we have discussed the two limiting cases, crystal-field excitations for dominant coupling to the lattice and collective orbital waves for dominant exchange interactions. Detailed theoretical predictions for the contribution of orbital waves to the optical conductivity would certainly be very helpful in order to experimentally distinguish between a predominantly local excitation and a collective mode. However, a quantitative description of experimental data will require to treat both the exchange interactions and the coupling to the lattice on an equal footing [79].

3. CI cluster calculations and the point-charge model

Thus far, no detailed predictions exist for the optical conductivity in the case of dominant exchange interactions. We thus compare our experimental data with the predictions for 'local' crystal-field excitations. CI cluster calculations have been performed for many years in order to assign the correct symmetry and orbital occupancy to d–d excitations (see, e.g. chapter 10 of [54]). A typical cluster consists of the transition-metal ion and the surrounding anions, e.g. $[TiO_6]^{9-}$. More distant ions are taken into account as point charges only. The following parameters are being used: (i) the Slater integrals, (ii) the local crystal field and (iii) the tight-binding parameters.

(i) The Slater integrals describe the full local electron–electron interactions which give rise to the main multiplet structure. They have been obtained from Hartree–Fock calculations for a bare ion [80]. Then, these values have been reduced to 80% in order to account for the neglect of the 4s shell.

(ii) The crystal field or Madelung potential represents the electrostatic potential of all ions within the crystal, which is assumed to be infinite. The ions are considered to be point charges.

[10] Here, we have used the term 'magnon' to denote spinons in spin chains, triplons in spin ladders and magnons in a long-range ordered antiferromagnet.

The crystal field controls the on-site energies and gives rise to the energy splitting between the orbitals. We have calculated the crystal field using an Ewald summation, i.e. the summation is partly performed in real space, partly in momentum space, and thus pertains to the infinite crystal. The orbital splitting depends on the local derivatives of the Madelung potential. Therefore, we expanded the Madelung potential in terms of spherical harmonics, which allows us to calculate the ionic crystal-field splitting if the expectation values of $\langle r^k \rangle$ are known [81], where r denotes the electron coordinate with respect to the transition-metal site and k the order of the expansion. These expectation values have been obtained from Hartree–Fock calculations [80].

(iii) The tight-binding parameters account for hopping processes between the ligands and the transition-metal ions [82, 83]. For many materials they are well known from fits to LDA band-structure calculations. Some general rules have been derived for the dependence of the parameters $pd\sigma$ and $pd\pi$ on the distance between two ions [82]. Finally, the values for the on-site Coulomb repulsion on the transition-metal site (U_{dd}) and on the ligands (U_{pp}) as well as the charge-transfer energy Δ have been taken as reported from core-level and photoemission spectroscopy [84]. The cluster calculations have been performed using the code XTLS8 by Tanaka [85].

In the case of the $3d^1$ Ti^{3+} compounds, we report both the crystal-field splitting arising from the electrostatic potential (indicated below as 'point-charge model') and the result of the cluster calculation including the hybridization with the ligands.

4. Experimental

Details concerning the crystal growth and characterization have been described in [86] for TiOCl, in [35, 87] for $RTiO_3$, in [88] for $LaMnO_3$, in [89, 90] for Y_2BaNiO_5, in [91] for $CaCu_2O_3$ and [92] for $K_4Cu_4OCl_{10}$.

Using a Fourier-transform spectrometer, we have measured the transmittance and reflectance in the energy range from 0.01 eV up to 3 eV at temperatures varying from 4 to 775 K. With the knowledge of both transmittance and reflectance, it is possible to directly calculate the complex optical conductivity $\sigma(\omega)$ [93]. For the transmittance measurements, the samples were polished on both sides. The reflectance was measured on samples with a thickness of $d \gtrapprox 1$ mm, which were polished on only one side to prevent a contribution from multiple reflections within the sample. In order to determine $\sigma(\omega)$ accurately, the thickness d of the samples used for the transmittance measurement must be chosen appropriately. Note that the transmittance depends exponentially on d [93]. For each compound studied here, transmittance data were collected on various samples with varying thickness d (e.g. ranging from 12.5 to 300 μm in case of $LaTiO_3$ and from 2 to 500 μm in $LaMnO_3$). Thick samples (d of the order of several 100 μm) are sensitive to weak absorption features ($\sigma < 1\,\Omega^{-1}\,\mathrm{cm}^{-1}$), but they become opaque for larger values of σ. Thinner samples allow us to determine larger values of σ, but in the range of weak absorption the spectra are dominated by Fabry-Perot interference fringes. Single crystalline samples with $d < 10\,\mu$m are difficult to handle. In particular, the surfaces of polished crystals are not absolutely parallel to each other, so that the thickness d may vary by a few μm across the sample. This significantly complicates a quantitative analysis of the data of very thin samples. A reliable analysis of transmittance data measured on thin single crystals is hence restricted to

values of $\sigma(\omega)$ smaller than about $100\,\Omega^{-1}\,\mathrm{cm}^{-1}$. For larger values of $\sigma(\omega)$, the transmittance has to be measured on thin films. Alternatively, a Kramers–Kronig analysis of the reflectance or ellipsometric techniques may be used. However, measuring the transmittance is essential for an accurate determination of weak absorption features such as d–d transitions.

Here, we focus on insulating samples. The accessible energy range for transmittance measurements is therefore limited by the strong absorption of fundamental phonon excitations below about 80 meV and by the steep rise of $\sigma(\omega)$ at the onset of excitations across the electronic gap.

5. Orbital excitations in TiOCl

Recently, TiOCl has been discussed as a novel inorganic spin-Peierls system [32, 33, 86], [94]–[102], [105]–[110]. Above ∼200 K, the magnetic susceptibility χ is well described by a model for a one-dimensional homogeneous $S = 1/2$ chain with exchange constant $J \approx 676\,\mathrm{K}$ [86]. At $T_{c1} = 67\,\mathrm{K}$, χ shows a transition to a non-magnetic ground state [32, 86]. However, indications for a second transition (or crossover) at $T_{c2} \approx 92\,\mathrm{K}$ are observed in the magnetic susceptibility [32, 86] as well as in NMR [95] and ESR data [86]. Strong fluctuations above $T_{c2} \approx 92\,\mathrm{K}$ were discussed on the basis of NMR [95], Raman and infrared data [96]–[98]. The phase transition at T_{c1} is generally interpreted as a spin-Peierls transition. This is corroborated by the observation of a doubling of the unit cell along the b direction below T_{c1} in x-ray scattering [101, 102]. However, the physics at higher temperatures and, in particular, the occurrence of a second phase transition have not been understood so far. It has been speculated [32, 86], [95]–[100] that this unconventional behaviour is caused by strong orbital fluctuations, assuming a near degeneracy of the t_{2g} subshell in this distorted structure.

The structure of TiOCl consists of buckled Ti–O bilayers separated by Cl ions. The bilayers are stacked along the c direction. The $[TiO_4Cl_2]$ octahedra are strongly distorted (see figure 4). In particular, they are strongly compressed along the x axis. At room temperature, the Ti–O bond lengths are 1.96 Å in x direction, whereas the bond lengths in the yz plane amount to 2.19 Å for the Ti–O bonds and 2.40 Å for the Ti–Cl bonds [103]. On each Ti site, the ground-state orbital has predominantly $y^2 - z^2$ character (see below), forming one-dimensional chains along the b (or y) direction. The space group is Pmmn at 300 K and $P2_1/m$ at 4 K [101]. There is no inversion symmetry on the Ti site, thus orbital excitations are directly infrared-active, i.e. they contribute to $\sigma(\omega)$ without the additional excitation of a phonon. In this case, the point-charge model does not only allow one to estimate the transition energies, but also the polarization dependence of the orbital excitations can be predicted (see equation (1)). In particular, strict polarization selection rules apply to the room-temperature structure (see table 1). Below T_{c1}, the distortions give rise to a mixing of the orbitals, hence the polarization selection rules are no longer strict. Nevertheless, it is possible to give some 'effective' selection rules because the dipole matrix elements for the main transitions are about three orders of magnitude (or more) larger than for the weak ones.

The transmittance measured on a thin single crystal of TiOCl is depicted in figure 5 for two polarization directions, $E \parallel a$ and $E \parallel b$. Unfortunately, measurements with $E \parallel c$ could not be performed since the available samples were very thin in the stacking direction. Our data are in agreement with unpolarized measurements reported for energies above 1.3 eV [104]. Above ∼2 eV, the sample is opaque due to excitations across the gap. The transmittance is strongly

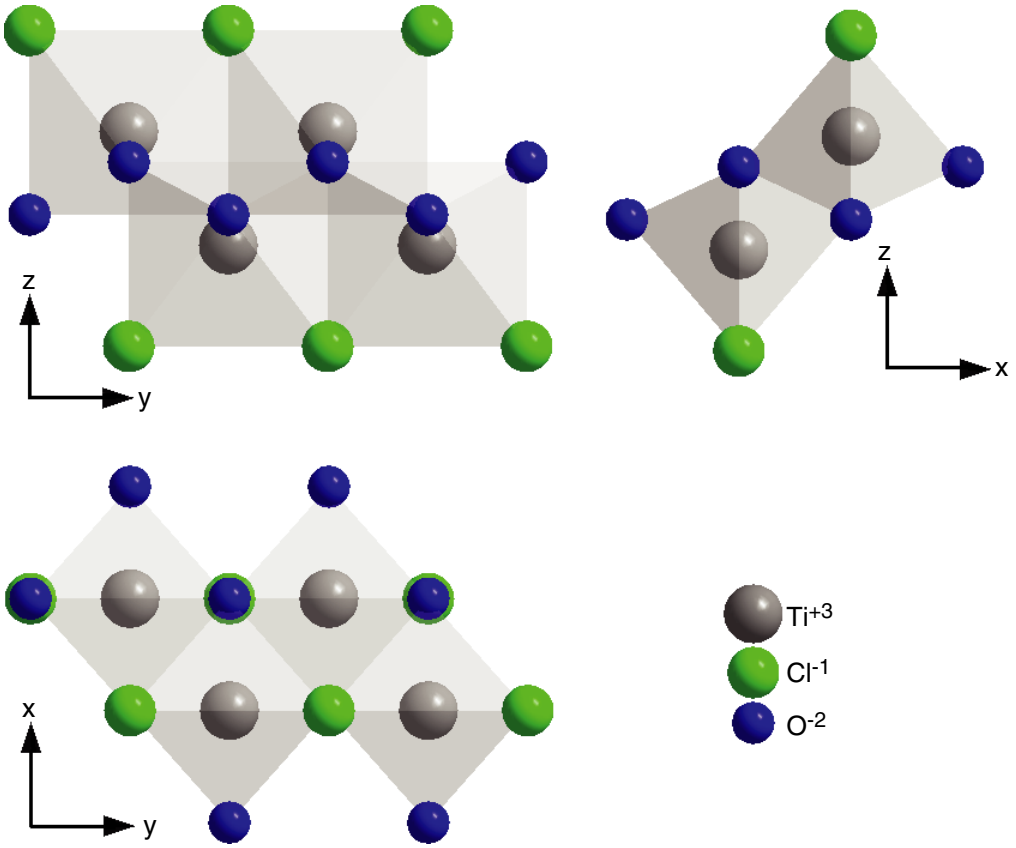

Figure 4. View along different axes on four strongly distorted $[TiO_4Cl_2]$ octahedra in TiOCl. The $S = 1/2$ chains are running parallel to the b axis. We use $x \parallel a$, $y \parallel b$ and $z \parallel c$. For convenience, we use these axes not only at 300 K, but also for the discussion of the 4 K data.

suppressed at 0.6–0.7 eV for $E \parallel a$ and at 1.5–1.6 eV for $E \parallel b$. The absorption feature at 0.65 eV appears as a weak dip also for $E \parallel b$, and the feature at 1.5 eV gives rise to a weak shoulder for $E \parallel a$. An interpretation in terms of phonons or magnetic excitations can be excluded at these energies. The excitation energies and, in particular, the polarization dependence are in good agreement with the results of the cluster calculation (see table 1). Thus these features can unambiguously be attributed to orbital excitations. As far as the polarization selection rules are concerned, the appearance of weak features in the other polarizations at 300 K can be attributed either to a small misalignment of the polarizer, to absorption due to the phonon-activated mechanism, or to a small admixture of xy character to the ground state (see below), e.g. by spin–orbit coupling or due to the dispersion (i.e. away from the Γ point). The absorption at about 1.5 eV shows an asymmetric profile with a steep drop of the transmittance on the low-energy side, in agreement with the expectations for phonon sidebands in case of small changes of the relaxed bond length (see figure 3). A precise determination of the line shape requires measurements on a thinner sample, in which the transmittance is not suppressed to zero. The data for $T = 4$ K and for 300 K are very similar, but the line width increases with increasing temperature.

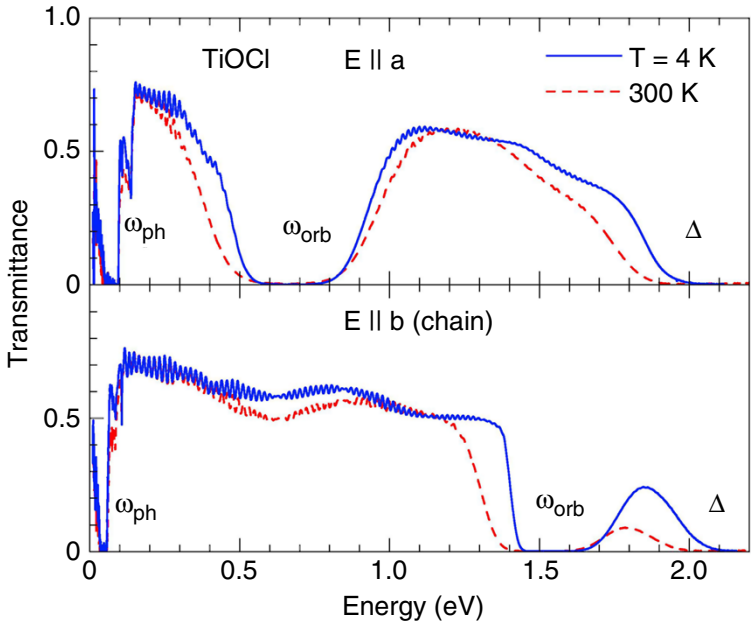

Figure 5. Transmittance spectra of TiOCl with phonon absorption below ≈0.1 eV, multiphonon peaks up to about 0.15 eV, orbital excitations at about 0.65 eV ($E \parallel a$) and 1.5 eV ($E \parallel b$), and the band gap $\Delta \approx 2$ eV. The periodic Fabry-Perot fringes in the highly transparent range indicate multiple reflections within the sample.

In the cluster calculation for TiOCl, we have to take into account the hybridization between the Ti ions and both, O as well as Cl ions. In comparison to, for instance, $LaTiO_3$ or $LaMnO_3$, we thus have two additional parameters, namely the charge-transfer energy Δ_{Cl} between Ti and Cl, and the Ti–Cl hybridization t_{Cl}. In fact, an accurate description of hybridization effects is essential in order to reproduce the splitting between the t_{2g} and e_g subshells. Due to the strong compression of the octahedra along the x direction, the electrostatic contribution of the point-charge model predicts that the lowest excited state has d_{yz} character, i.e. belongs to the e_g subshell[11]. At the same time, the polarization selection rules given in table 1 predict for 300 K that this transition to the d_{yz} level (with a small admixture of y character) can be observed for $E \parallel b$. Experimentally, the corresponding absorption feature for $E \parallel b$ is found at about 1.5 eV, i.e. more than 1 eV higher than predicted by the point-charge model. However, the energy of this transition can be described correctly by taking into account the hybridization between Ti and its ligands, which typically adds more than 1 eV to the splitting between t_{2g} and e_g subshells.

The parameters $U_{dd} = 4$ eV, $\Delta_O = 5$ eV and $\Delta_{Cl} = 3$ eV are estimated following the LDA+U results of [99]. The orbital excitation energies depend only weakly on U_{dd}. In order to model the relative strength of the Ti–O and the Ti–Cl hybridization, we have to consider the larger ionic radius of Cl compared to O (r_{Cl}–$r_O \approx 0.4$ Å) as well as the larger polarizability. For the former, we assume that the hybridization is the same for the two ligands if the bond length

[11] The ligands are located approximately along the diagonals of the yz plane, hence d_{yz} denotes a state from the e_g subshell.

Table 1. Crystal-field splitting of $3d^1$ Ti^{3+} in TiOCl and polarization dependence for infrared absorption at 300 and 4 K. Comparison of experimental data (see figure 5) and theoretical results obtained using the point-charge model and a cluster calculation (see section 3). The cluster calculation uses $U_{dd} = 4$ eV, $\Delta_O = 5$ eV, $\Delta_{Cl} = 3$ eV and an enhancement of the Ti–Cl hybridization by $t^* = 1.3$ (see text). The calculations are based on the 300 K structure reported in [103] and on the 4 K data in [101]. At 4 K, there are two inequivalent Ti sites. For convenience, we use $x \parallel a$, $y \parallel b$ and $z \parallel c$ at both temperatures. All energies are given in eV. At 300 K, the given polarization selection rules are strict. Due to the lower symmetry at 4 K, only 'effective' selection rules survive in the sense that the dipole matrix elements for the 'main' transitions indicated at 4 K are about three orders of magnitude (or more) larger than those not given in the table.

Theory					
Character	$y^2 - z^2$	xy	xz	yz	$3x^2 - r^2$
Admixture (300 K)	z	–	x	y	z
Main admixture (4 K)	y, z	x	x	y, z	y, z
Point charge (300 K)	0	0.39	0.68	0.34	1.28
Cluster (300 K)	0	0.25	**0.69**	**1.24**	2.11
Cluster (4 K, Ti_a)	0	0.26	**0.73**	**1.53**	2.20
Cluster (4 K, Ti_b)	0	0.25	**0.77**	**1.47**	2.18
Polarization (300 K)		–	$E \parallel a$	$E \parallel b$	$E \parallel c$
Main polarization (4 K)		$E \parallel a$	$E \parallel a$	$E \parallel b, c$	$E \parallel b, c$
Experimental					
Energy		–	**0.65**	**1.5**	–
Polarization		–	$E \parallel a$	$E \parallel b$	–

equals $r_{Ti} + r_X$ (X = O and Cl). Additionally, the larger polarizability of Cl compared to O is modelled by a factor t^* by which the Ti–Cl hybridization is further enhanced. Good agreement between the calculated energies and the experimental results at both temperatures is obtained for $t^* \approx 1.3$ (see table 1)[12].

The energy of the lowest excited state (xy orbital) is crucial in order to determine whether orbital fluctuations are the correct explanation for the interesting physics observed in TiOCl. In the room-temperature structure, the transition to the first excited state is not directly infrared-active, but it becomes directly infrared-active in the distorted low-temperature structure below T_{c1}. According to our cluster calculation, the lowest excited state is expected at about 0.2–0.25 eV. However, our infrared data do not show a distinct absorption feature in this range (see figure 5). A rough estimate of the spectral weight can be obtained from the point-charge model, which predicts that the dipole matrix element at 4 K is about one order of magnitude smaller than for the transition to the xz orbital. Due to a factor of $1/\omega$, this means that the spectral weight of the excitations to the xy and to the xz orbital should be comparable in $\sigma(\omega)$.

[12] Enhancing t_{Cl} by t^* is necessary in order to push the d_{yz} level (from the e_g subshell) up to 1.5 eV. With increasing t^*, the energy of the d_{yz} orbital increases strongly, whereas the energies of d_{xy} and d_{xz} (from the t_{2g} subshell) decrease. For $t^* = 1$ we find the following excitation energies: 0.32, 0.79, 1.32 and 2.21 eV at 4 K for the site labelled Ti_a in table 1.

One possible explanation for the lack of a corresponding feature in our infrared data is that the first and the second excited states are nearly degenerate, as indicated by band-structure results [32, 99].

The scenario of strong orbital fluctuations assumes a near degeneracy of the $y^2 - z^2$ and xy states. However, a sizeable admixture of the state with xy character to the ground state would have drastic consequences for the selection rules. A transition from xy to $xz + x(yz + y)$ will give rise to absorption for $E \parallel b$ ($E \parallel a$), i.e. just the opposite of the selection rules derived for the transitions from the $y^2 - z^2$ state. This may explain the weak features at about 0.65 eV for $E \parallel b$ and 1.5 eV for $E \parallel a$, but at the same time the weakness of these features compared to the strong absorption in the perpendicular direction puts a severe limit to the admixture of xy character to the ground state. Moreover, the g factor observed in ESR spectroscopy is close to 2 [86], which indicates that the orbital moment is quenched by a significant splitting ($\geqslant 0.2$ eV) within the t_{2g} subshell. A sizeable splitting of the t_{2g} subshell is in agreement with recent LDA+U and LDA+DMFT results [108]–[110]. However, the degree of orbital polarization still needs to be clarified. In [108], the lowest orbital ($y^2 - z^2$ in our notation) is populated by only 70%, indicating the possible importance of interorbital fluctuations, whereas a population with 0.98 electrons was reported in [109].

Both our cluster calculation and, in particular, the observed polarization dependence show that there is no significant admixture of the xy orbital to the ground state. Thus orbital fluctuations are clearly suppressed. In order to understand the interesting physics of TiOCl, it is therefore sufficient to consider the interplay of lattice and spin degrees of freedom. We suggest that the occurrence of two-phase transitions results from the frustration of interchain interactions in this peculiar bilayer structure [107].

The remarkable splitting of 0.65 eV of the t_{2g} subshell is caused by the strong distortions of the $[TiO_4Cl_2]$ octahedra and by the different charges on O and Cl sites within an octahedron. This large splitting clearly shows that t_{2g} systems are not necessarily good model compounds for the study of orbital effects based on (near) orbital degeneracy within the ground state.

6. Orbital excitations in $RTiO_3$ (R = La, Sm and Y)

One of the novel quantum phenomena proposed in the field of orbital physics are orbital liquids, in which long-range orbital order is suppressed by quantum fluctuations [19]–[22]. Based on neutron scattering results, the $3d^1$ pseudo-cubic perovskite $LaTiO_3$ has been discussed as a realization of an orbital liquid [21, 31]. In comparison to compounds with e_g electrons, t_{2g} systems are promising candidates for interesting orbital phenomena due to the threefold orbital degeneracy and due to the smaller coupling to the lattice. However, the results for TiOCl discussed above also show that the splitting of the t_{2g} subshell can be significant. In $LaTiO_3$, a detailed study of the structure revealed a sizeable distortion of $\approx$3%, lifting the orbital degeneracy [35]. At this stage, it is heavily debated whether $LaTiO_3$ represents an orbital liquid [21, 31], [35]–[49]. The scenario of an orbital liquid requires that the reduction of the ground-state energy by quantum fluctuations is larger than the energy splitting of the orbitals due to the distortion. A study of the orbital excitations and the determination of the excitation energies are very interesting in this context.

In $RTiO_3$, the magnetic ordering changes as a function of the ionic radius of the R ions from antiferromagnetic for R = La to ferromagnetic for R = Y. Within the orbital-liquid model, it has

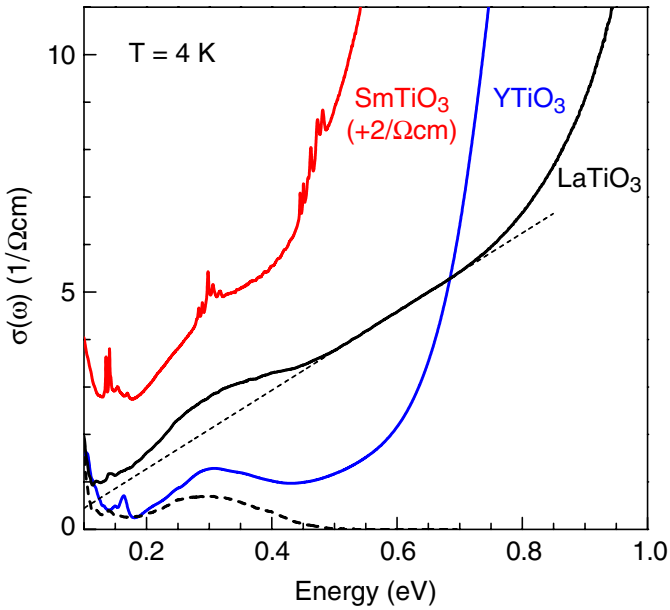

Figure 6. Optical conductivity of (twinned) single crystals of $LaTiO_3$, $SmTiO_3$ and $YTiO_3$ at $T = 4$ K. An offset of $2\,\Omega^{-1}\,cm^{-1}$ has been added to the data of $SmTiO_3$ for clarity. Phonon-activated orbital excitations are observed at 0.3 eV in all three compounds. For $LaTiO_3$, an estimate of the orbital excitation band has been obtained by subtracting a linear background (- - - -). The additional sharp features in $SmTiO_3$ at 0.15, 0.3 and 0.45 eV are due to crystal-field transitions within the Sm 4f shell [111].

been proposed that the transition from antiferromagnetic order to ferromagnetic order should define a quantum critical point. $SmTiO_3$ is still antiferromagnetic, but lies close to the critical value of the ionic radius [113]. By measuring both the transmittance and the reflectance on twinned single crystals, we were able to observe phonon-activated orbital excitations in $LaTiO_3$, $SmTiO_3$ and $YTiO_3$ at about 0.3 eV, i.e. in the frequency range between the phonons and the band gap (see figure 6). In $YTiO_3$, the Hubbard gap can be identified with the onset of strong absorption at about 0.6 eV. In $LaTiO_3$, the optical conductivity shows strong absorption above 0.8 eV, but an absorption tail extends down to about 0.2 eV. In a recent LDA+DMFT study, the Hubbard gap of $LaTiO_3$ ($YTiO_3$) was reported to be 0.3 eV (1 eV) [48]. This issue of the onset of interband excitations will be discussed elsewhere. Here, we focus on the weak absorption features at about 0.3 eV observed in $LaTiO_3$, $SmTiO_3$ and $YTiO_3$.

An interpretation in terms of phonons can be excluded since phonon absorption is restricted to below ≈80 meV. The small peak in $YTiO_3$ at about 160 meV typically marks the upper limit for two-phonon absorption in transition-metal oxides with perovskite structure [51]. Absorption of three or more phonons has to be much weaker. According to the magnon energies observed by inelastic neutron scattering [31, 114], the energy of 0.3 eV is much too high also for phonon-assisted magnetic absorption (i.e. two magnons plus a phonon [72, 73]). The very sharp additional absorption lines observed in $SmTiO_3$ at about 0.15, 0.3 and 0.45 eV are attributed to crystal-field transitions within the Sm 4f shell [111]. These lines are much narrower than the d–d bands, because in case of the 4f levels both the coupling to the lattice and the coupling between nearest-neighbour sites are much smaller.

Table 2. Crystal-field splitting of $3d^1$ Ti^{3+} in $LaTiO_3$, $SmTiO_3$ and $YTiO_3$ as calculated in the point-charge model and in a cluster calculation ($U_{dd} = 4\,eV$, $\Delta = 4\,eV$). All values are given in eV. For comparison with the optical conductivity data in figure 6, the energy of the symmetry-breaking phonon has to be added.

La					
Point charge	0	0.21	0.23	0.9	1.0
Cluster	0	0.24	0.26	2.2	2.4
Sm					
Point charge	0	0.15	0.26	0.9	1.0
Cluster	0	0.21	0.31	2.2	2.5
Y					
Point charge	0	0.14	0.28	0.9	1.0
Cluster	0	0.19	0.33	2.2	2.4

Our interpretation of the features at about 0.3 eV, in terms of orbital excitations, is strongly corroborated by Raman scattering data of $LaTiO_3$ and $YTiO_3$. A detailed analysis of the Raman data can be found in [112]. The Raman spectra show similar features as the optical conductivity but shifted to lower energies by 50–70 meV. As discussed above, d–d transitions have even parity and are thus Raman active, whereas a contribution to $\sigma(\omega)$ arises only due to the simultaneous excitation of a phonon breaking the inversion symmetry on the transition-metal site. The observed shift of 50–70 meV is in good agreement with the energies of the Ti–O bond-bending and bond-stretching phonon modes, which are expected to yield the dominant contributions (see section 2). Moreover, the transition probability for such a multiparticle excitation ('orbiton' plus phonon) is small, in agreement with the small absolute value of $\sigma(\omega)$.

We thus conclude that the orbital nature of the features is unambiguous. The orbital excitation energy amounts to about 0.2–0.25 eV (without the symmetry-breaking phonon). The central issue is whether these features reflect the collective nature of orbital fluctuations [71] or whether they have to be interpreted as local crystal-field excitations. In principle, both the superexchange coupling between the orbitals and the coupling of the orbitals to the lattice will contribute to the excitations, thus the question has to be addressed on a quantitative level. Theoretical treatments which take into account both kinds of coupling on an equal footing clearly would be very interesting.

At this stage, such calculations are not available. Thus we focus on a comparison of our data with the results for local crystal-field excitations obtained within the point-charge model and a cluster calculation (see section 3). We have used the structural data of [35] for $LaTiO_3$, of [113] for $SmTiO_3$ and of [115] for $YTiO_3$. As discussed for TiOCl, the point-charge model underestimates the splitting between the t_{2g} and e_g subshells by more than 1 eV. At the same time, the predictions of the point-charge model and of the cluster calculation for the splitting of the t_{2g} subshell are rather similar, with a maximum difference of 0.06 eV. We find good agreement between theory and experiment concerning the peak energy of 0.2–0.25 eV in all three compounds (see table 2). Similar values for the t_{2g} splitting result from a recent LDA+DMFT study, in which the covalency between R and O ions has been identified as the driving force for the distortions [48]. Significantly smaller values (27 and 181 meV for $YTiO_3$; 54 and 93 meV for $LaTiO_3$) have been derived from tight-binding fits of the t_{2g} band structure [49]. On the basis of x-ray absorption and spin-resolved

photoemission data of $LaTiO_3$, it has been concluded that the splitting between the ground state and the lowest excited state is about 0.1–0.3 eV [37]. Our results for TiOCl (see above) show that 0.2–0.25 eV is not an extraordinarily large value for the t_{2g} splitting of a $3d^1$ Ti^{3+} compound.

The above-mentioned change of the magnetic ordering pattern as a function of the ionic radius of the R ions is accompanied by a change in the character of the distortions [113]. The radius of the Sm^{3+} ions is close to the critical value [113]. One thus may hope to find a smaller crystal-field splitting in $SmTiO_3$. In contrast, the orbital fluctuation model predicts that the orbital excitations for not too low energies are very similar across the quantum critical point [71], in agreement with the experimental result. Our calculations predict that the splitting between the first and the second excited states increases from La via Sm to Y. However, the energies are not as sensitive to the radius of the R ions as one may have expected, and we consider these small differences as smaller than the absolute uncertainty of the calculation. Moreover, the experimental features are too broad and too close in energy to the excitations across the gap in order to test this prediction.

Within the crystal-field scenario, the large line width can be explained by the coupling to the lattice, i.e. in terms of the Franck–Condon effect (see section 2). The additional excitation of a symmetry-breaking phonon in the infrared measurements may give rise to an additional broadening in $\sigma(\omega)$ as compared to the Raman data.

At the present stage, the orbital excitation energy and the observed distortions [35] can be described satisfactorily within a local crystal-field scenario, in which the t_{2g} splitting is dominated by the coupling to the lattice. On the basis of our optical conductivity data, we did not find any clear evidence for strong orbital fluctuations. Also the isotropic spin-wave dispersion of $LaTiO_3$ observed in inelastic neutron scattering [31] can be explained within a crystal-field scenario [116, 117]. The small ordered moment may result from the combination of quantum fluctuations within the spin channel, spin–orbit coupling and the small Hubbard gap. The latter gives rise to enhanced fluctuations both in the charge and in the orbital channel and thus may contribute significantly to the reduction of the ordered moment [118][13].

Nevertheless, the uncertainty of the theoretical predictions for the crystal-field splitting is too large to rule out a finite contribution from orbital fluctuations. The energy of 0.2–0.25 eV is certainly too high for a one-orbiton excitation in a collective-mode scenario. However, it possibly can be reconciled with two-orbiton excitations [71], or with the sum of crystal-field and fluctuation contributions. Additional information can be derived from the Raman data. The resonance behaviour and the polarization dependence yield evidence for a collective nature of the orbital excitations in $RTiO_3$ [112]. Detailed predictions for the energy and the line shape of orbitons in the optical conductivity are necessary to further clarify this issue.

7. Orbitons versus multiphonon peaks in $LaMnO_3$

In the manganites, the orbital degree of freedom certainly plays an important role [119]. In contrast to the threefold degeneracy of the t_{2g}^1 configuration of Ti^{3+} ions, the $t_{2g}^3e_g^1$ configuration of Mn^{3+} ions is doubly degenerate within the e_g orbitals in a cubic environment. The degeneracy can be lifted by both a collective Jahn–Teller effect and by orbital interactions. In $LaMnO_3$, orbital

[13] At the same time, this is the central idea behind the orbital liquid scenario: the small gap gives rise to strong orbital fluctuations which in turn reduce the spin order [21].

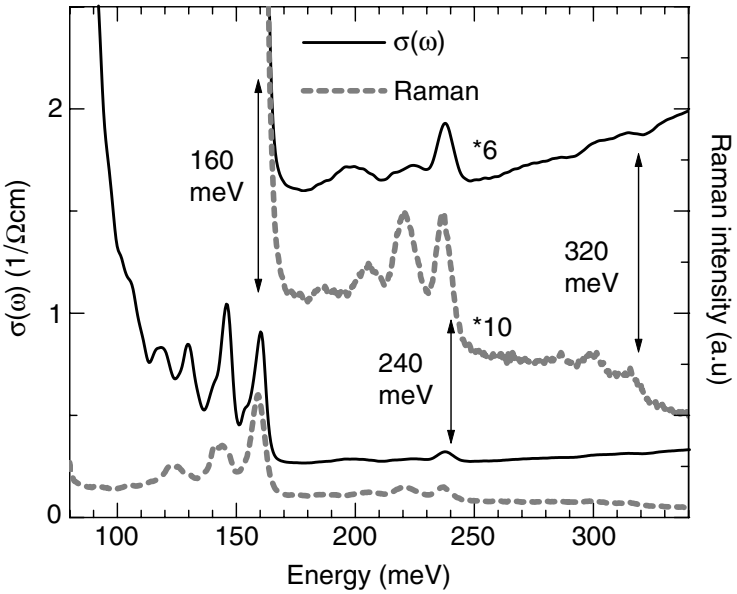

Figure 7. Optical conductivity $\sigma(\omega)$ ($T = 4$ K) of $LaMnO_3$ [51] showing multiphonon features at, e.g. two, three and four times 80 meV. For comparison, we plot the Raman-scattering data ($T = 15$ K) by Choi *et al* [125]. The two top curves focusing on the high-energy features show the same data multiplied by a factor of 6 and 10, respectively.

order has been observed below $T_{OO} = 780$ K [120]–[122]. In order to explain the existence of orbital order at temperatures above the spin ordering temperature, it is necessary to invoke the Jahn–Teller effect. It has been proposed that the experimentally observed orbital ordering pattern can be explained by taking into account anharmonicity [123].

Raman scattering data reported for orbitally ordered $LaMnO_3$ have been interpreted as the first experimental evidence for the existence of orbitons [26]. This claim is based on the observation of three Raman lines at 126, 144 and 160 meV, on their temperature dependence and on the analysis of the polarization dependence. Since Raman spectroscopy is restricted to $k = 0$ excitations, it is not possible to follow the dispersion of the elementary excitations. However, in the case of $LaMnO_3$, one expects different excitation branches with different symmetries at $k = 0$, and these were identified with the three Raman lines [26]. We have challenged the orbiton interpretation on the basis of a comparison with the optical conductivity spectrum [51] (see also [126]).

In $LaMnO_3$, the direct observation of orbital excitations is allowed in Raman spectroscopy, but a contribution to $\sigma(\omega)$ requires to break the parity selection rule, e.g. via the simultaneous excitation of a phonon. Therefore, the orbital excitations are expected to be shifted in $\sigma(\omega)$ with respect to the Raman lines by a phonon energy of roughly 50–80 meV (see section 2 and [124]), in agreement with the results for $RTiO_3$ discussed in the preceding section.

We have determined $\sigma(\omega)$ very accurately in the relevant frequency range (see figure 7) by measuring both the transmittance of thin (twinned) single crystalline platelets and the reflectance of a sample with $d \approx 1$ mm (figure 8). The small spectral weight of the various features observed in figure 7 at energies above ~80 meV, i.e. above the range of fundamental phonon absorption, is typical for multiphonon spectra in insulating transition-metal oxides. For comparison, see

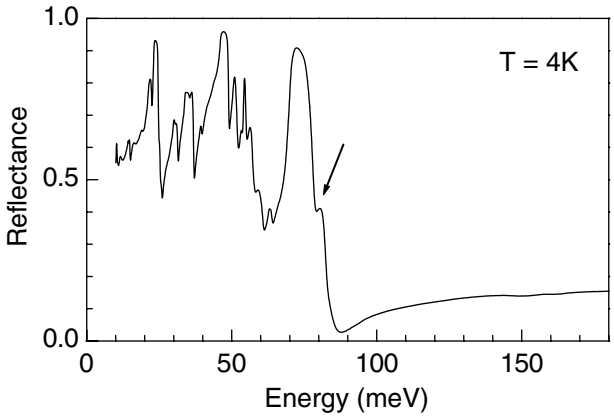

Figure 8. Reflectance spectrum of $LaMnO_3$ in the phonon range. The highest phonon mode is observed at 80 meV, as indicated by the arrow.

e.g. the spectra of $\sigma(\omega)$ of $RTiO_3$, Y_2BaNiO_5 or $CaCu_2O_3$ in the present work or of $LaCoO_3$ in [51].

In $\sigma(\omega)$ we find absorption features at about 118, 130, 146 and 160 meV which are very similar to the three Raman lines mentioned above. Moreover, we identify some weak features at about 240 and 320 meV. At the latter two energies, very similar features have been observed in Raman scattering[14] on the same samples by Choi *et al* [125] (see figure 7), using a surface that had been polished for the transmittance measurement. The highest infrared-active fundamental phonon mode is observed in the reflectance data at about 80 meV (see figure 8 and [126, 127]). It has been interpreted as a zone-boundary Mn–O bond-stretching mode which is folded back to $k = 0$ in the orbitally ordered state [126]. A weak Raman line has been found at the same frequency [53, 125]. Given the existence of a fundamental mode at 80 meV, the features at 160, 240 and 320 meV are naturally explained as two-, three- and four-phonon modes, respectively. In particular, the Raman line at 160 meV is certainly not too high in energy for a two-phonon mode. At 160 meV, similar two-phonon features are observed also in other pseudo-cubic perovskites such as $LaCoO_3$ [51] or $YTiO_3$ (see figure 6). Three-phonon Raman scattering in $LaMnO_3$ at room temperature and above has been reported recently in the range 210–250 meV [53]. Multiphonon Raman scattering is predicted to be strong in orbitally ordered $LaMnO_3$ due to the Franck–Condon effect [128] (see figure 3).

Let us briefly address the issue of selection rules and the problems for a theoretical description of multiphonon features. The symmetry of a multiphonon mode has to be derived using the multiplication rules of the irreducible representations of the contributing fundamental modes. Thus an overtone of a forbidden fundamental mode may very well be allowed. Peaks within the two- or multiphonon continua reflect a high density of states and do not necessarily correspond to simple multiples of $k = 0$ phonon modes. A precise theoretical treatment of the two- and multiphonon continua requires a detailed knowledge of the dispersion of the fundamental modes throughout the entire Brillouin zone. Unfortunately, such a detailed analysis of neutron scattering data has failed so far due to the twinning of the samples [129]. Moreover, multiphonon

[14] The Raman measurements have been performed by Choi *et al* at the RWTH Aachen, Germany [125]. The Raman data have been obtained in a quasi-backscattering geometry using a laser energy of 2.34 eV (Ar^+ laser).

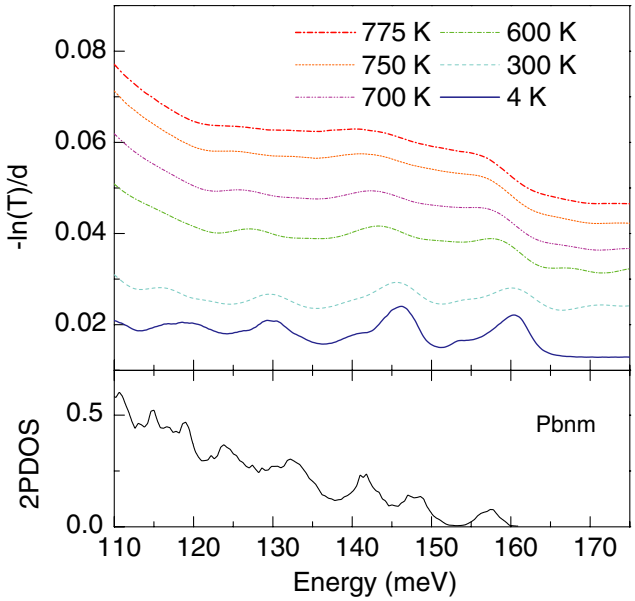

Figure 9. Top: temperature dependence of the multiphonon features in $LaMnO_3$. Plotting $-\ln(T)/d$, where T is the transmittance and d the sample thickness, yields an estimate of the absorption coefficient [93]. The curves have been shifted vertically for clarity. Bottom: the $k = 0$ part of the two-phonon density of states calculated for $LaMnO_3$ in Pbnm symmetry [129].

features may depend strongly on the sample quality and on details of the sample growth [130], which strongly complicates a meaningful comparison with theory. The bottom panel of figure 9 shows the $k = 0$ part of the two-phonon density of states calculated for $LaMnO_3$ in Pbnm symmetry[15]. The calculation is based on a shell model [131], the parameters have been deduced from similar perovskite compounds where the lattice dynamics was studied in detail. The highest two-phonon peak is predicted slightly below 160 meV, the overall structure is in reasonable agreement with the optical data.

Within the orbiton interpretation, an explanation of features at the same energy (e.g. 160 meV) in Raman and infrared spectroscopy requires to break the parity-selection rule without the simultaneous excitation of a phonon. This can in principle be achieved by impurities, but the phonon mechanism lined out above turns out to be much more effective [54]. Roughly speaking, a small impurity concentration of, e.g., 1% breaks the selection rule only at a small percentage of sites, whereas the phonon is effective throughout the entire sample. This is corroborated by the shift between the Raman and the infrared data observed in $RTiO_3$ (see above). Moreover, the remaining differences between the Raman and the infrared spectra—e.g. the peak energies of 126 and 144 meV as compared to 118, 130 and 146 meV—can easily be attributed in the multiphonon case to the different selection rules, giving different weights to the two-phonon density of states. However, the orbiton scenario including impurities to account for the parity selection rule predicts identical peak energies in both spectroscopies.

[15] The calculations of the two-phonon density of states have been performed by W Reichardt (FZ Karlsruhe, Germany).

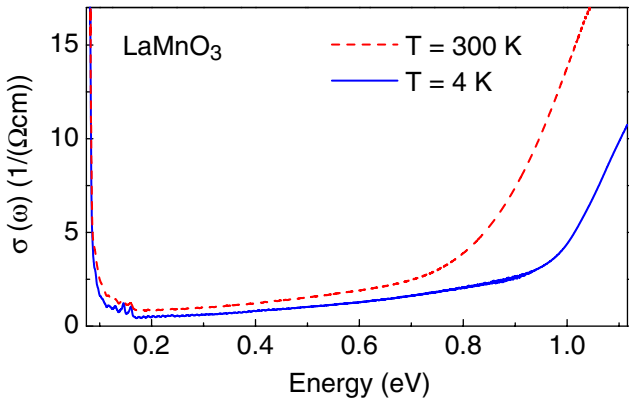

Figure 10. Optical conductivity $\sigma(\omega)$ of $LaMnO_3$ in the energy range from phonon absorption to the onset of excitations across the Mott gap.

One argument favouring the orbiton interpretation was the disappearance of the relevant Raman lines upon heating above the orbital ordering temperature $T_{OO} = 780$ K [26]. We have measured the transmittance of $LaMnO_3$ at temperatures up to 775 K (see figure 9), the highest temperature available in our experimental setup. The room-temperature spectra before and after heating to 775 K are identical, showing that the oxygen content of the sample did not change significantly upon heating. The absorption bands in the range of 120–160 meV broaden strongly with increasing temperature, but they clearly persist also at 775 K, i.e. close to T_{OO}. The sensitivity of the Raman lines [26, 125] indicates that these multiphonon lines are Raman-forbidden in the high-temperature structure and become Raman-allowed due to the symmetry change across the phase transition.

We have tried very carefully to find the orbital excitations at higher energies by investigating the transmittance of several different samples of $LaMnO_3$, varying the thickness between 2 and 500 μm. Transmittance measurements on a thick sample are sensitive to very weak absorption features, whereas thin samples are better suited for the determination of larger values of $\sigma(\omega)$ (see section 4). Our data do not show any absorption band between the multiphonon range and the onset of excitations across the Mott gap at about 1 eV [132, 133] (see figure 10).

Allen and Perebeinos [134] predicted a strong orbital absorption band centred around 2 eV with a Gaussian envelope of vibrational sidebands starting at about 1 eV. Additionally, they predicted a strong temperature dependence close to the onset of absorption, in agreement with our data. A detailed comparison between theory and experiment requires a precise determination of the line shape to still higher frequencies, i.e. measurements on still thinner samples.

In comparison with our data of orbital excitations observed in other transition-metal oxides presented in this paper, the results on $LaMnO_3$ strongly suggest that the orbital excitations are pushed to energies above 1 eV due to the rather strong Jahn–Teller effect in this e_g electron system. Theoretical estimates of the splitting vary between 0.7 and 2 eV [134]–[140]. In a cluster calculation, we have obtained a ground state quintuplet, while the two lowest excited states are triplets lying at 1.3 and 1.8 eV, respectively (for $U = 7.5$ eV and $\Delta = 4.5$ eV [84]). Our calculation predicts the lowest quintuplet, which corresponds to the splitting of the e_g subshell, at about 1.9 eV. Recently, a Jahn–Teller splitting of the order of 2 eV was derived from resonant Raman scattering data [52, 53]. A large Jahn–Teller splitting is also in agreement with the absence of low-energy orbiton features in inelastic x-ray data [70].

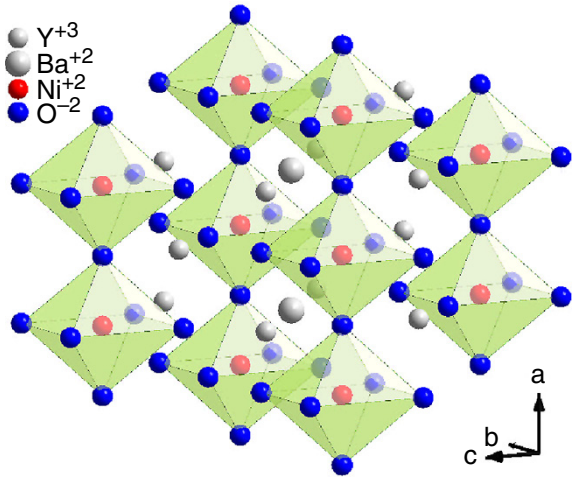

Figure 11. Crystal structure of Y_2BaNiO_5 with $S = 1$ chains running along the a axis.

The eigenmodes show a mixed character (phonon–orbiton) if the coupling to the lattice (Jahn–Teller effect) and the orbital exchange interactions are taken into account on an equal footing [79]. In [125], the coupling between phonons and orbitons is discussed on the basis of the changes observed in the (multi-)phonon Raman spectra upon variation of temperature, symmetry or doping level. An interpretation of the Raman features at about 160 meV in terms of phonon–orbiton mixed modes with predominantly orbiton character requires a rather small value for the electron–lattice coupling [79]. However, if the Jahn–Teller splitting is large ($\gtrsim$1 eV), the spectrum recovers the shape predicted by the Franck–Condon effect (see figure 3) [79]. Note that increasing the coupling to the lattice results not only in a blue shift of the excitation energy but also in a suppression of the orbital band width.

In summary, our search for orbital excitations below the Mott gap was not successful in $LaMnO_3$. We are convinced that undoped $LaMnO_3$ is not a good model system for the study of orbital waves.

8. Y_2BaNiO_5

The compound Y_2BaNiO_5 is an example of a Haldane system, an antiferromagnetic $S = 1$ chain with an energy gap between the collective spin-singlet ground state and the lowest-excited triplet state. The exchange coupling constant has been determined by neutron scattering, $J \approx 21$ meV [141, 142]. The chains are formed by corner-sharing NiO_6 octahedra (see figure 11) and run along the a axis. The Ni–O distance is only 1.89 Å parallel to the chains, whereas it amounts to 2.19 Å perpendicular to the chains. Thus the octahedra are strongly compressed.

The optical conductivity as determined from transmittance and reflectance measurements is shown in figure 12 for two polarization directions, $E \parallel a$ and $E \parallel b$. In figure 13 we plot the spectra below 1 eV on an enlarged scale. Several broad peaks are observed between 0.34 and $\approx$2.5 eV in both polarization directions, and the spectra display a pronounced polarization dependence. As in the other compounds discussed above, phonons are limited to energies below about 80 meV. A magnetic origin can also be ruled out, since phonon-activated magnetic excitations are expected

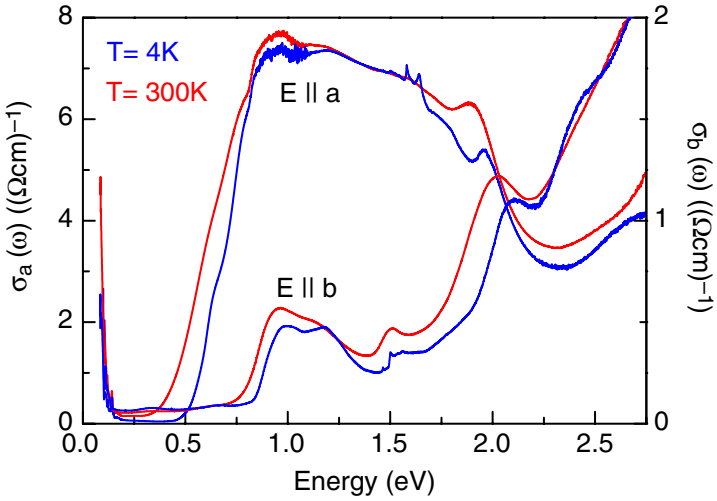

Figure 12. Optical conductivity of Y_2BaNiO_5 for polarization of the electric field vector parallel to the *a* axis (left scale) and to the *b* axis (right scale), respectively.

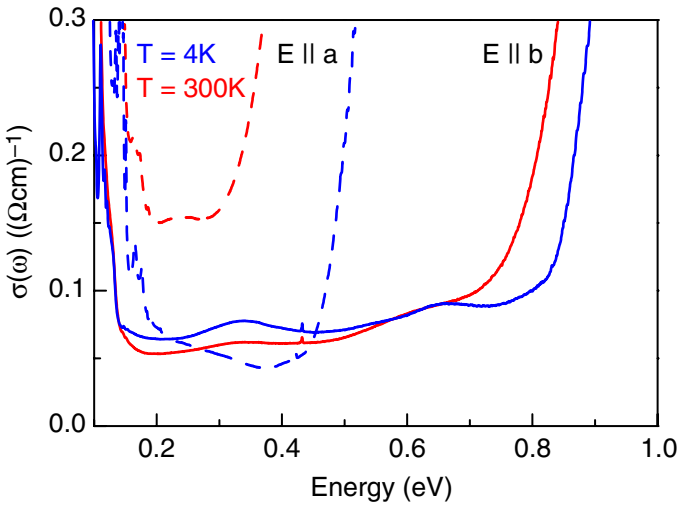

Figure 13. Optical conductivity of Y_2BaNiO_5 at low energies on an enlarged scale (cf figure 12).

to peak below 0.2 eV for a $S = 1$ chain with $J \approx 21$ meV [143] (including a phonon contribution of 80 meV). We did not succeed in separating a possible phonon-activated magnetic contribution from the multiphonon continuum in this frequency range. The transparency of the crystals indicates that the electronic excitations have a large gap. The features between 0.34 and 2.5 eV can thus be attributed to orbital excitations. The rather complex structure of the spectra reflects the large number of multiplets of the $3d^8$ Ni^{2+} ions in this compound.

In order to confirm this interpretation, we calculated the crystal-field levels using a cluster calculation. Here we used $U_{dd} = 7.0$ eV, $U_{pp} = 5.0$ eV and $\Delta = 3$ eV [84, 85]. The effect of varying U_{dd} between 6 and 8 eV and Δ between 2 and 4 eV is shown for a few selected levels in figure 14. The energy levels hardly depend on the precise value of U_{dd}, whereas the influence

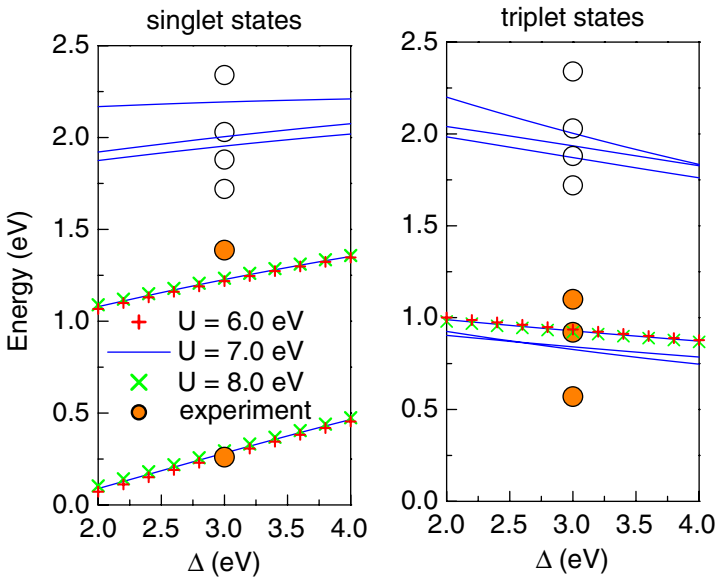

Figure 14. Crystal-field levels of the $3d^8$ Ni^{2+} ions in Y_2BaNiO_5 as a function of Δ as obtained in a cluster calculation. The dependence on U_{dd} (6–8 eV) is shown for a few selected levels. The splitting of the triplet states by spin–orbit coupling is not shown for clarity. Circles denote the experimentally determined peak positions (cf figures 12 and 13). For comparison between experiment and theory, the phonon energy of 50–80 meV still has to be added to the calculated values. Below 1.5 eV, the singlet/triplet character of the experimental peaks has been identified (●). Above 1.5 eV, the energy levels are too close for an unambiguous identification (○).

of Δ is more significant. All spin-singlet energies rise with increasing Δ whereas the spin-triplet energies decrease. For $U_{dd} = 7.0$ eV and $\Delta = 3$ eV, the cluster calculation predicts spin-singlet states at 0.28, 1.23, 1.95, 2.00 and 2.19 eV, and spin-triplet states at 0.83, 0.84, 0.93, 1.87, 1.94 and 2.00 eV, respectively. Here, we have neglected the splitting of the triplets ($\lesssim$50 meV) by spin–orbit coupling for simplicity. Since the ground state has triplet character, the transitions to the singlet states are forbidden by the spin selection rule $\Delta S = 0$. Comparing with the experimental data, one can identify the lowest two singlet states with the very weak absorption band at 0.34 eV ($E \parallel b$, see figure 13) and with the sharp features at about 1.5 eV. Note that the phonon energy of 50–80 meV still has to be added to the calculated values. The finite absorption strength of the feature at 0.34 eV is attributed to spin–orbit coupling, the sharp peaks at 1.5 eV are addressed below. The three peaks at about 0.65, 1.0 and 1.2 eV are assigned to the lowest three triplet states. The overall agreement between the calculated energy levels and the observed peak frequencies is reasonable.

In the following, we want to focus on the two lowest spin-singlet states. The first excited singlet state at 0.34 eV may serve as an example for a low-energy orbital excitation in a distorted crystal structure. Its low energy arises from competing interactions. On the one hand, the Coulomb interactions prefer a parallel alignment of the spins of the two holes in the 3d shell (Hund's rule), which forces the two holes to occupy different orbitals in the ground state (predominantly the $3z^2 - r^2$ and the xy orbitals, which both point towards the negatively charged O ligands in this

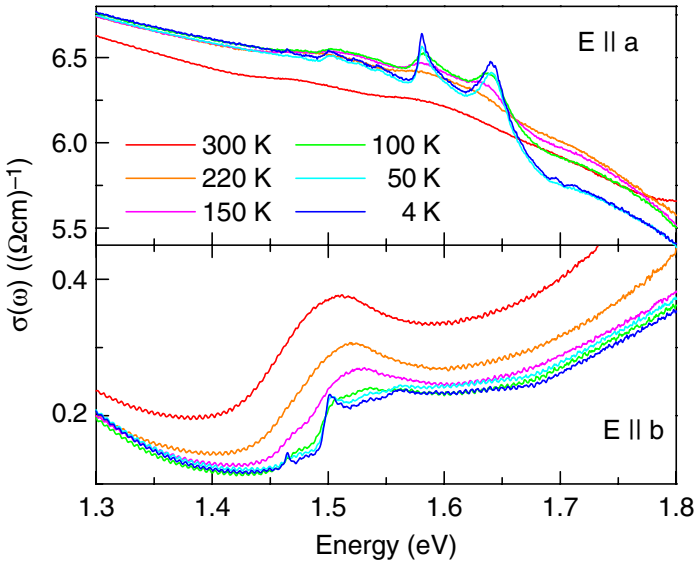

Figure 15. Temperature dependence of the transition to the second excited spin-singlet state in Y_2BaNiO_5. The sinusoidal structure is due to Fabry-Perot interference fringes in the transmittance data (cf figure 5).

compound). On the other hand, the crystal field and the Ni–O hybridization give rise to a large splitting of these two orbitals due to the strong compression of the octahedra, favouring the $3z^2-r^2$ orbital (in the present case, the dominant contribution arises from the hybridization). Therefore, the singlet state with both holes predominantly occupying the $3z^2-r^2$ orbital is not much higher in energy than the spin-triplet ground state. Increasing the Ni–O hybridization by applying external pressure may lead to a further reduction of the singlet energy.

The transition to the second singlet state at about 1.5 eV can roughly be understood as a pure spin-flip transition, i.e. this state shows nearly the same orbital occupancy as the triplet ground state. This explains the very narrow line width compared to all other absorption bands, since the lattice hardly reacts to the spin flip (see the discussion of the Franck–Condon principle in figure 3). The fine structure is attributed to magnetic dipole transitions and to magnon-assisted electric dipole transitions [58, 67, 68]. A more detailed polarization analysis with additional measurements on a different sample surface is required in order to determine whether the absorption features depend on the direction of the magnetic-field component or on the electric-field component. The temperature dependence of the sharp features at about 1.5 eV is shown in figure 15. The fine structure is rapidly washed out with increasing temperature, which is attributed to the loss of coherence of the magnetic excitations.

9. $CaCu_2O_3$ and $K_4Cu_4OCl_{10}$

These two cuprate compounds show interesting magnetic properties. For the purpose of the present paper, they serve as examples for crystal-field excitations at high energies. In the undoped parent compounds of the high-T_c superconducting cuprates, predictions for the lowest crystal-field excitation ($x^2-y^2 \rightarrow 3z^2$) varied between 0.6 [144] and 1.9 eV [145] in semi-empirical and *ab initio* cluster calculations [144]–[147]. Experimental evidence supporting low-lying

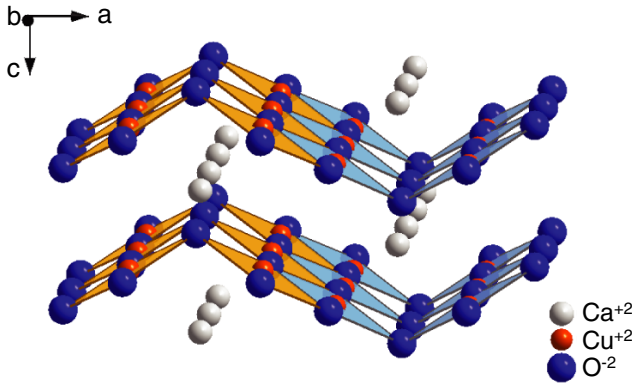

Figure 16. Crystal structure of $CaCu_2O_3$ [150].

d–d excitations was reported on the basis of optical conductivity data [76, 148] with a possible relevance for the mechanism of high-T_c superconductivity. However, the corresponding features at about 0.3–0.5 eV in $\sigma(\omega)$ have been interpreted successfully in terms of phonon-assisted magnetic absorption by Lorenzana and Sawatzky [72, 73]. By means of inelastic x-ray scattering [149] and optical third-harmonic generation [65], evidence for a splitting between the $x^2 - y^2$ ground state and the $3z^2$ orbital of 1.6–2 eV has been derived.

The crystal structure of $CaCu_2O_3$ shows buckled Cu_2O_3 layers which are stacked along the c direction [150] (see figure 16). Magnetically, the system is strongly anisotropic, with a dominant antiferromagnetic coupling between the Cu spins parallel to the b axis, and weak couplings in the perpendicular directions ($J_b \gg J_a \approx J_c$) [63, 151]. The weak 3D coupling gives rise to long-range order below $T_N \approx 25$ K. The interlayer distance amounts to 3.7 Å, and the local environment of the $3d^9$ Cu^{2+} ions is close to a square of four O ions. The local symmetry on the Cu site deviates only slightly from D_4 symmetry. In D_4 symmetry, the hole occupies the $x^2 - y^2$ orbital, and the xy orbital constitutes the first excited state, whereas the $3z^2$ orbital shows the highest energy of the 3d orbitals. In a cluster calculation we find the first excited state at 1.3 eV.

We have determined the optical conductivity from reflectance and transmittance data (see figure 17). Lorenzana–Sawatzky-type phonon-assisted magnetic excitations were observed at about 0.4 eV [63]. The onset of excitations across the charge-transfer gap is observed at about 1.2–1.3 eV. The feature at 1.1 eV is attributed to a crystal-field excitation. At 300 K, both the onset of charge-transfer excitations and the crystal-field exciton peak are smeared out significantly.

The compound $K_4Cu_4OCl_{10}$ has been found in volcanic sedimentations. The crystal structure is shown in figure 18 [92]. It shows Cu_4 tetrahedra with a single O ion in the centre of each tetrahedron (see figure 18). Each Cu^{2+} ion carries a spin of $S = 1/2$ and is surrounded by a $[Cl_4O]$ cage (see figure 19). The tetrahedra are well separated by K and Cl ions. This compound thus represents in good approximation a zero-dimensional model system for the study of local crystal-field excitations.

As far as the magnetism is concerned, one expects two degenerate spin-singlet states for a regular, undistorted $S = 1/2$ tetrahedron. The degeneracy can be lifted by magnetic quantum fluctuations between coupled tetrahedra. The dynamics of such geometrically frustrated quantum spin systems with low-lying singlet excitations have attracted considerable interest [152]–[155].

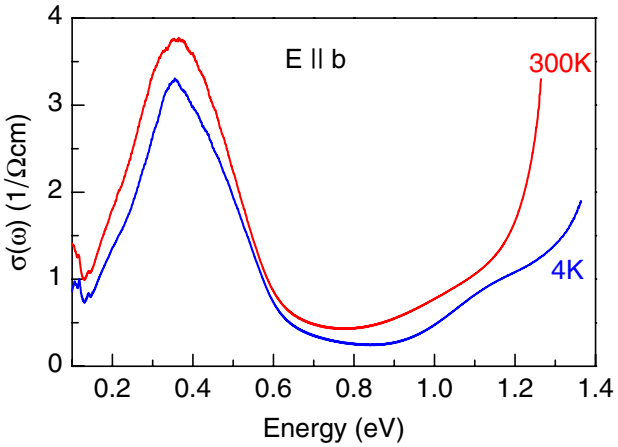

Figure 17. Optical conductivity of $CaCu_2O_3$, showing phonon-assisted magnetic excitations around 0.4 eV [63], the charge-transfer gap at about 1.3 eV and a d–d exciton just below the gap.

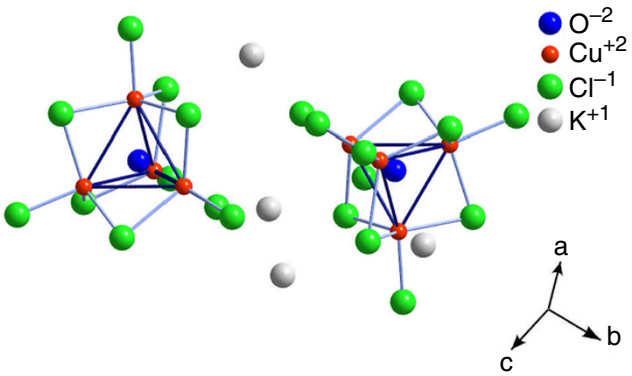

Figure 18. Crystal structure of $K_4Cu_4OCl_{10}$ [92].

However, the degeneracy can also be lifted by distortions of the tetrahedra, similar to the competition between orbital quantum fluctuations and lattice distortions described above.

We have measured the transmittance T of a polycrystalline sample that was compressed in a KBr pellet because $K_4Cu_4OCl_{10}$ is sensitive to moisture. Plotting $-\ln T$ yields an estimate of the absorption, as stated above [93]. The Cu–O bond-stretching mode is split into three distinct absorption peaks (see left panel of figure 20), indicating a distortion of the tetrahedra and a suppression of the magnetic quantum fluctuations.

Crystal-field excitations have been observed at 1.22 and 1.47 eV (see figure 20). The background is attributed to scattering on grain boundaries which increases with increasing energy. For an estimate of the crystal-field splitting, we consider a $CuOCl_4$ cluster as shown in figure 19. Using the same parameters as for TiOCl (in particular $t^* = 1.3$, see above), we obtain four excited states at 1.3, 1.5, 1.8 and 1.9 eV above the ground state. A further increase of t^* hardly affects the two lower energies, but pushes the two higher levels beyond 2 eV, in reasonable agreement with the experimental result.

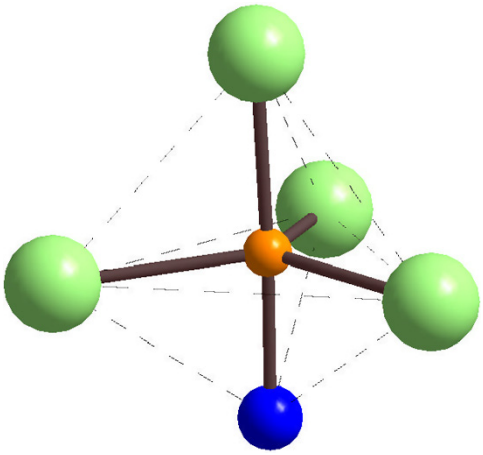

Figure 19. The $CuOCl_4$ cluster considered for the calculation of the crystal-field splitting in $K_4Cu_4OCl_{10}$.

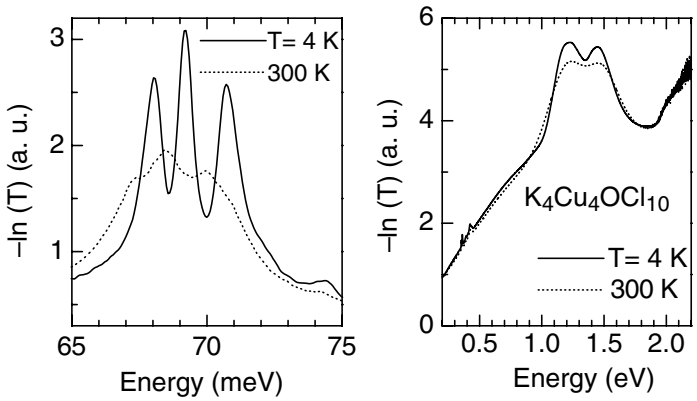

Figure 20. Negative logarithm of the transmittance of a polycrystalline sample compressed in KBr. Left: splitting of the Cu–O bond-stretching phonon. Right: crystal-field excitations.

10. Conclusion

Orbital excitations have been observed in the optical conductivity of a series of transition-metal compounds. The orbital excitations gain a finite spectral weight in $\sigma(\omega)$ either due to the absence of inversion symmetry on the transition-metal site, a phonon-activated mechanism, or magnon-exciton sidebands. In general, reasonable agreement has been obtained between the observed peak energies and the predictions of a cluster calculation. In the case of TiOCl, also the experimentally observed polarization dependence can be understood very well within the point-charge model. Here, the lack of inversion symmetry on the Ti site allows to make strict predictions for the polarization dependence in the room-temperature structure, i.e. each transition is expected only in one particular polarization. A pronounced polarization dependence has also been observed in the case of phonon-activated absorption bands of Y_2BaNiO_5. However, most of these bands are observed both for $E \parallel a$ and $E \parallel b$, i.e. only the intensity is changing as a function of polarization.

At the present stage, our optical conductivity data do not yield clear evidence for a collective nature of the orbital excitations in any of the compounds studied here. The energetically lowest orbital excitations were observed in Y_2BaNiO_5 (0.34 eV) and in $RTiO_3$ (0.3 eV). In Y_2BaNiO_5, the low energy can be explained by the competition between Hund's rule coupling (favouring a spin-triplet state, in which the two holes on a $3d^8$ Ni^{2+} ion occupy different orbitals) and Ni–O hybridization (favouring a spin-singlet state with both holes in the $3z^2$ orbital due to the strong compression of the octahedra). In the case of $RTiO_3$, detailed theoretical predictions for $\sigma(\omega)$ concerning, e.g., the peak energy and the line shape for absorption of collective orbital fluctuations are called for. In particular, a quantitative estimate of the possible importance of orbital fluctuations can only be derived from our data if the orbital exchange interactions and the coupling to the lattice are treated on an equal footing. However, the resonance behaviour and the polarization dependence of the Raman data [112] give evidence for a collective nature of the orbital excitations in $RTiO_3$. In TiOCl, on the other hand, the t_{2g} splitting was found to be about 0.65 eV. A scenario of strong orbital fluctuations with a significant admixture of the xy orbital to the ground state is in contradiction with the observed polarization dependence. We thus consider a dominant role of orbital fluctuations in this compound as very unlikely.

Acknowledgments

We acknowledge the fruitful collaborations with C Ulrich, B Keimer, K-Y Choi, P Lemmens and G Güntherodt regarding the Raman measurements on $RTiO_3$ and $LaMnO_3$. We are indebted to W Reichardt for provision of the calculated two-phonon density of states of $LaMnO_3$. We thank A Tanaka for the use of his program XTLS8, and A Gössling, D I Khomskii, E Müller-Hartmann, L H Tjeng, G S Uhrig and in particular G Khaliullin for many stimulating discussions. This project is supported by the DFG via SFB 608.

References

[1] Imada M, Fujimori A and Tokura Y 1998 *Rev. Mod. Phys.* **70** 1039
[2] Tokura Y and Nagaosa N 2000 *Science* **288** 462
[3] Auerbach A 1994 *Interacting Electrons and Quantum Magnetism* (New York: Springer)
[4] Gogolin A O, Nersesyan A A and Tsvelik A M 1998 *Bosonization and Strongly Correlated Systems* (Cambridge: Cambridge University Press)
[5] Hohenberg P C 1967 *Phys. Rev.* **158** 383
[6] Mermin N D and Wagner H 1966 *Phys. Rev. Lett.* **22** 1133
[7] Barnes T, Dagotto E, Riera J and Swanson E S 1993 *Phys. Rev.* B **47** 3196
[8] Haldane F D M 1983 *Phys. Rev. Lett.* **50** 1153
[9] Faddeev L D and Takhtajan L A 1981 *Phys. Lett.* A **85** 375
[10] Andrei N and Lowenstein J H 1979 *Phys. Rev. Lett.* **43** 1698
[11] Karbach M, Müller G, Bougourzi A H, Fledderjohann A and Mütter K-H 1997 *Phys. Rev.* B **55** 12510
[12] Arai M, Fujita M, Motokawa M, Akimitsu J and Bennington S M 1996 *Phys. Rev. Lett.* **77** 3649
[13] Schmidt K P and Uhrig G S 2003 *Phys. Rev. Lett.* **90** 227204
[14] Sushkov O P and Kotov V N 1998 *Phys. Rev. Lett.* **81** 1941
[15] Windt M, Grüninger M, Nunner T, Knetter C, Schmidt K P, Uhrig G S, Kopp T, Freimuth A, Ammerahl U, Büchner B and Revcolevschi A 2001 *Phys. Rev. Lett.* **87** 127002
[16] Dagotto E, Riera J and Scalapino D 1992 *Phys. Rev.* B **45** 5744
[17] Dagotto E 1999 *Rep. Prog. Phys.* **62** 1525

[18] Uehara M, Nagata T, Akimitsu J, Takahashi H, Môri N and Kinoshita K 1996 *J. Phys. Soc. Japan* **65** 2764
[19] Ishihara S, Yamanaka M and Nagaosa N 1997 *Phys. Rev.* B **56** 686
[20] Feiner L F, Oles A M and Zaanen J 1997 *Phys. Rev. Lett.* **78** 2799
[21] Khaliullin G and Maekawa S 2000 *Phys. Rev. Lett.* **85** 3950
[22] Khaliullin G 2001 *Phys. Rev.* B **64** 212405
[23] Khaliullin G, Horsch P and Oleś A M 2001 *Phys. Rev. Lett.* **86** 3879
[24] Sirker J and Khaliullin G 2003 *Phys. Rev.* B **67** 100408(R)
[25] Horsch P, Khaliullin G and Oleś A M 2003 *Phys. Rev. Lett.* **91** 257203
[26] Saitoh E, Okamoto S, Takahashi K T, Tobe K, Yamamoto K, Kimura T, Ishihara S, Maekawa S and Tokura Y 2001 *Nature* **410** 180
[27] Ishihara S, Inoue J and Maekawa S 1997 *Phys. Rev.* B **55** 8280
[28] Khaliullin G and Okamoto S 2002 *Phys. Rev. Lett.* **89** 167201
[29] Khaliullin G and Okamoto S 2003 *Phys. Rev.* B **68** 205109
[30] Ishihara S 2004 *Phys. Rev.* B **69** 075118
[31] Keimer B, Casa D, Ivanov A, Lynn J W, von Zimmermann M, Hill J P, Gibbs D, Taguchi Y and Tokura Y 2000 *Phys. Rev. Lett.* **85** 3946
[32] Seidel A, Marianetti C A, Chou F C, Ceder G and Lee P A 2003 *Phys. Rev.* B **67** 020405(R)
[33] Seidel A and Lee P A 2004 *Phys. Rev.* B **69** 094419
[34] Ulrich C, Khaliullin G, Sirker J, Reehuis M, Ohl M, Miyasaka S, Tokura Y and Keimer B 2003 *Phys. Rev. Lett.* **91** 257202
[35] Cwik M, Lorenz T, Baier J, Müller R, André G, Bourée F, Lichtenberg F, Freimuth A, Schmitz R, Müller-Hartmann E and Braden M 2003 *Phys. Rev.* B **68** 060401(R)
[36] Craco L, Laad M S, Leoni S and Müller-Hartmann E 2004 *Phys. Rev.* B **70** 195116
[37] Haverkort M W, Hu Z, Tanaka K, Ghiringhelli G, Roth H, Cwik M, Lorenz T, Schüßler-Langeheine C, Streltsov S V, Mylnikova A S, Anisimov V I, de Nadai C, Brookes N B, Hsieh H H, Lin H-J, Chen C T, Mizokawa T, Taguchi Y, Tokura Y, Khomskii D I and Tjeng L H 2005 *Phys. Rev. Lett.* **94** 056401
[38] Mochizuki M and Imada M 2001 *J. Phys. Soc. Japan* **70** 2872
[39] Mochizuki M and Imada M 2003 *Phys. Rev. Lett.* **91** 167203
[40] Mochizuki M and Imada M 2004 *J. Phys. Soc. Japan* **73** 1833
[41] Mochizuki M and Imada M 2004 *New J. Phys.* **6** 154
[42] Fritsch V, Hemberger J, Eremin M V, Krug von Nidda H-A, Lichtenberg F, Wehn R and Loidl A 2002 *Phys. Rev.* B **65** 212405
[43] Hemberger J, Krug von Nidda H-A, Fritsch V, Deisenhofer J, Lobina S, Rudolf T, Lunkenheimer P, Lichtenberg F, Loidl A, Bruns D and Büchner B 2003 *Phys. Rev. Lett.* **91** 066403
[44] Kiyama T and Itoh M 2003 *Phys. Rev. Lett.* **91** 167202
[45] Harris A B, Yildirim T, Aharony A, Entin-Wohlmann O and Korenblit I Ya 2003 *Phys. Rev. Lett.* **91** 087206
[46] Harris A B, Yildirim T, Aharony A, Entin-Wohlmann O and Korenblit I Ya 2004 *Phys. Rev.* B **69** 035107
[47] Kikoin K, Entin-Wohlmann O, Fleurov V and Aharony A 2003 *Phys. Rev.* B **67** 214418
[48] Pavarini E, Biermann S, Poteryaev A, Liechtenstein A I, Georges A and Andersen O K 2004 *Phys. Rev. Lett.* **92** 176403
[49] Solovyev I V 2004 *Phys. Rev.* B **69** 134403
[50] Fang Z and Nagaosa N 2004 *Phys. Rev. Lett.* **93** 176404
[51] Grüninger M, Rückamp R, Windt M and Freimuth A 2002 *Nature* **418** 39
[52] Krüger R, Schulz B, Naler S, Rauer R, Budelmann D, Bäckström J, Kim K H, Cheong S-W, Perebeinos V and Rübhausen M 2004 *Phys. Rev. Lett.* **92** 097203
[53] Martín-Carrón L and de Andrés A 2004 *Phys. Rev. Lett.* **92** 175501
[54] Ballhausen C F 1962 *Introduction to Ligand Field Theory* (New York: McGraw-Hill)
[55] Kikoin K A and Fleurov V N 1994 *Transition Metal Impurities in Semiconductors. Electronic Structure and Physical Properties* (Singapore: World Scientific)
[56] Nelson E D, Wong J Y and Schawlow A L 1967 *Phys. Rev.* **156** 298

[57] Schawlow A L, Wood D L and Clogston A M 1959 *Phys. Rev. Lett.* **3** 271
[58] Sell D D, Greene R L and White R M 1967 *Phys. Rev.* **158** 489
[59] Hasan M Z, Isaacs E D, Shen Z-X, Miller L L, Tsutsui K, Tohyama T and Maekawa S 2000 *Science* **288** 1811
[60] Khaliullin G and Kilian R 2000 *Phys. Rev.* B **61** 3494
[61] van den Brink J, Stekelenburg W, Khomskii D I, Sawatzky G A and Kugel K I 1998 *Phys. Rev.* B **58** 10276–82
[62] Figgis B N and Hitchman M A 1999 *Ligand Field Theory and its Applications* (New York: Wiley)
[63] Grüninger M, Windt M, Benckiser E, Nunner T S, Schmidt K P, Uhrig G S and Kopp T 2003 *Adv. Solid State Phys.* **43** 95
[64] Falck J P, Perkins J D, Levy A, Kastner M A, Graybeal J M and Birgeneau R J 1994 *Phys. Rev.* B **49** 6246
[65] Schumacher A B, Dodge J S, Carnahan M A, Kaindl R A, Chemla D S and Miller L L 2001 *Phys. Rev. Lett.* **87** 127006
[66] Fromme B, Möller M, Anschütz T, Bethke C and Kisker E 1996 *Phys. Rev. Lett.* **77** 1548
[67] Ferguson J, Guggenheim H J and Tanabe Y 1966 *J. Phys. Soc. Japan* **21** 692
[68] Cador O, Mathonière C and Kahn O 2000 *Inorg. Chem.* **39** 3799–804
[69] Guillaume M, Henggeler W, Furrer A, Eccleston R S and Trounov V 1995 *Phys. Rev. Lett.* **74** 3423
[70] Tanaka Y, Baron A Q R, Kim Y-J, Thomas K J, Hill J P, Honda Z, Iga F, Tsutsui S, Ishikawa D and Nelson C S 2004 *New J. Phys.* **6** 161
[71] Khaliullin G private communication
[72] Lorenzana J and Sawatzky G A 1995 *Phys. Rev. Lett.* **74** 1867
[73] Lorenzana J and Sawatzky G A 1995 *Phys. Rev.* B **52** 9576
[74] Suzuura H, Yasuhara H, Furusaki A, Nagaosa N and Tokura Y 1996 *Phys. Rev. Lett.* **76** 2579
[75] Lorenzana J and Eder R 1997 *Phys. Rev.* B **55** R3358
[76] Perkins J D, Graybeal J M, Kastner M A, Birgeneau R J, Falck J P and Greven M 1993 *Phys. Rev. Lett.* **71** 1621
[77] Perkins J D, Birgeneau R J, Graybeal J M, Kastner M A and Kleinberg D S 1998 *Phys. Rev.* B **58** 9390
[78] Perkins J D, Kleinberg D S, Kastner M A, Birgeneau R J, Endoh Y, Yamada K and Hosoya S 1995 *Phys. Rev.* B **52** R9863
[79] van den Brink J 2001 *Phys. Rev. Lett.* **87** 217202
[80] Cowan R D 1981 *The Theory of Atomic Structure and Spectra* (Berkeley, CA: University of California Press)
[81] Sugano S, Tanabe Y and Kamimura H 1970 *Multiplets of Transition-Metal Ions in Crystals* (New York: Academic)
[82] Harrison W A 1980 *Electronic Structure and the Properties of Solids* (San Francisco: Freeman)
[83] Slater J C and Koster G F 1954 *Phys. Rev.* **94** 1498
[84] Saitoh T, Bocquet A E, Mizokawa T and Fujimori A 1995 *Phys. Rev.* B **52** 5419
[85] Tanaka A and Jo T 1994 *J. Phys. Soc. Japan* **63** 2788
[86] Kataev V, Baier J, Möller A, Jongen L, Meyer G and Freimuth A 2003 *Phys. Rev.* B **68** 140405
[87] Lichtenberg F, Widmer D, Bednorz J G, Williams T and Reller A 1991 *Z. Phys.* B **82** 211
[88] Geck J, Wochner P, Kiele S, Klingeler R, Revcolevschi A, von Zimmermann M and Büchner B 2004 *New J. Phys.* **6** 152
[89] Massarotti V, Capsoni D, Bini M, Altomare A and Moliterni A G G 1999 *Z. Krist.* **214** 205
[90] Sulewski P E and Cheong S-W 1994 *Phys. Rev.* B **50** 551
[91] Sekar C, Ruck K, Krabbes G, Teresiak A and Watanabe T 2002 *Physica* C **378** 678
[92] de Boer J J, Bright D and Helle J N 1972 *Acta Crystallogr.* B **28** 3436
[93] Grüninger M, Windt M, Nunner T, Knetter C, Schmidt K P, Uhrig G S, Kopp T, Freimuth A, Ammerahl U, Büchner B and Revcolevschi A 2002 *J. Phys. Chem. Solids* **63** 2167–73
[94] Beynon R J and Wilson J A 1993 *J. Phys.: Condens. Matter* **5** 1983
[95] Imai T and Chou F C 2003 *Preprint* cond-mat/0301425
[96] Lemmens P, Choi K-Y, Caimi G, Degiorgi L, Kovaleva N N, Seidel A and Chou F C 2004 *Phys. Rev.* B **70** 134429

[97] Caimi G, Degiorgi L, Kovaleva N N, Lemmens P and Chou F C 2004 *Phys. Rev.* B **69** 125108
[98] Caimi G, Degiorgi L, Lemmens P and Chou F C 2004 *J. Phys.: Condens. Matter* **16** 5583
[99] Saha-Dasgupta T, Valenti R, Rosner H and Gros C 2004 *Europhys. Lett.* **67** 63
[100] Hemberger J, Hoinkis M, Klemm M, Sing M, Claessen R, Horn S and Loidl A 2005 *Preprint* cond-mat/0501517
[101] Shaz M, van Smaalen S, Palatinus L, Hoinkis M, Klemm M, Horn S and Claessen R 2005 *Phys. Rev.* B **71** 100405 (R)
[102] Abel E, Matan K, Chou F C and Lee Y S 2004 *Bull. Amer. Phys. Soc.* **49** 317 (*APS March Meeting Montreal 2004, Session D25.014*)
[103] Snigireva E M, Troyanov S I and Rybakov V B 1990 *Zh. Neorg. Khim.* **35** 1945 (ICSD code 39314)
[104] Maule C H, Tothill J N, Strange P and Wilson J A 1988 *J. Phys. C: Solid State Phys.* **21** 2153–79
[105] Lemmens P, Choi K-Y, Valenti R, Saha-Dasgupta T, Abel E, Lee Y S and Chou F C 2005 *Preprint* cond-mat/0501577
[106] Sasaki T, Mizumaki M, Kato K, Watabe Y, Nishihata Y, Takata M and Akimitsu J 2005 *Preprint* cond-mat/0501691
[107] Rückamp R, Baier J, Kriener M, Haverkort M W, Lorenz T, Uhrig G S, Jongen L, Möller A, Meyer G and Grüninger M 2005 *Preprint* cond-mat/0503409
[108] Craco L, Laad M and Müller-Hartmann E 2004 *Preprint* cond-mat/0410472
[109] Saha-Dasgupta T, Lichtenstein A and Valenti R 2005 *Phys. Rev.* B **71** 153108
[110] Pisani L and Valenti R 2005 *Phys. Rev.* B **71** 180409
[111] Barba D, Jandl S, Nekvasil V, Maryško M, Diviš M, Martin A A, Lin C T, Cardona M and Wolf T 2001 *Phys. Rev.* B **63** 054528
[112] Ulrich C, Gössling A, Grüninger M, Guennou M, Roth H, Cwik M, Lorenz T, Khaliullin G and Keimer B 2005 *Preprint* cond-mat/0503106
[113] MacLean D A, Ng H-N and Greedan J E 1979 *J. Solid State Chem.* **30** 35
[114] Ulrich C, Khaliullin G, Okamoto S, Reehuis M, Ivanov A, He H, Taguchi Y, Tokura Y and Keimer B 2002 *Phys. Rev. Lett.* **89** 167202
[115] Zubkov V G, Berger I F, Artamonova A M and Bazuyev G V 1984 *Kristallografiya* **29** 494–7
[116] Schmitz R, Entin-Wohlman O, Aharony A, Harris A B and Müller-Hartmann E 2004 *Preprint* cond-mat/0411583
[117] Schmitz R, Entin-Wohlman O, Aharony A, Harris A B and Müller-Hartmann E 2005 *Phys. Rev.* B **71** 144412
[118] Held K, Ulmke M, Blümer N and Vollhardt D 1997 *Phys. Rev.* B **56** 14469
[119] van den Brink J, Khaliullin G and Khomskii D I 2002 *Preprint* cond-mat/0206053
[120] Murakami Y, Hill J P, Gibbs D, Blume M, Koyama I, Tanaka M, Kawata H, Arima T, Tokura V, Hirota K and Endoh Y 1998 *Phys. Rev. Lett.* **81** 582
[121] Rodriguez-Carvajal J, Hennion M, Moussa F, Moudden A H, Pinsard L and Revcolevschi A 1998 *Phys. Rev.* B **57** R3189
[122] Chatterji T, Fauth F, Ouladdiaf B, Mandal P and Ghosh B 2003 *Phys. Rev.* B **68** 052406
[123] van den Brink J 2004 *New J. Phys.* **6** 201
[124] Reichardt W and Braden M 1999 *Physica* B **263–264** 416
[125] Choi K Y, Lemmens P, Güntherodt G, Pashkevich Y G, Gnezdilov V P, Reutler P, Pinsard-Gaudart L, Büchner B and Revcolevschi A 2005 *Preprint* cond-mat/0503460
[126] Saitoh E, Okamoto S, Tobe K, Yamamoto K, Kimura T, Ishihara S, Maekawa S and Tokura Y 2002 *Nature* **418** 40
[127] Paolone A, Roy P, Pimenov A, Loidl A, Mel'nikov O K and Shapiro A Y 2000 *Phys. Rev.* B **61** 11255
[128] Perebeinos V and Allen P B 2001 *Phys. Rev.* B **64** 085118
[129] Reichardt W and Braden M private communication
[130] Grüninger M, van der Marel D, Damascelli A, Zibold A, Geserich H P, Erb A, Kläser M, Wolf T, Nunner T and Kopp T 1999 *Physica* C **317–318** 286–91
[131] Chaplot S L, Reichardt W, Pintschovius L and Pyka N 1995 *Phys. Rev.* B **52** 7230

[132] Tobe K, Kimura T, Okimoto Y and Tokura Y 2001 *Phys. Rev.* B **64** 184421
[133] Kovaleva N N, Boris A V, Bernhard C, Kulakov A, Pimenov A, Balbashov A M, Khaliullin G and Keimer B 2004 *Phys. Rev. Lett.* **93** 147204
[134] Allen P B and Perebeinos V 1999 *Phys. Rev. Lett.* **83** 4828
[135] Millis A J 1996 *Phys. Rev.* B **53** 8434
[136] Pickett W E and Singh D J 1996 *Phys. Rev.* B **53** 1146
[137] Solovyev I, Hamada N and Terakura K 1996 *Phys. Rev.* B **53** 7158
[138] Elfimov I S, Anisimov V I and Sawatzky G A 1999 *Phys. Rev. Lett.* **82** 4264
[139] Ahn K H and Millis A J 2000 *Phys. Rev.* B **61** 13545
[140] Bala J and Oles A M 2000 *Phys. Rev.* B **62** R6085
[141] Darriet J and Regnault L P 1993 *Solid State Commun.* **86** 409
[142] Xu G, Aeppli G, Bisher M E, Broholm C, DiTusa J F, Frost C D, Ito T, Oka K, Paul R L, Takagi H and Treacy M M J 2000 *Science* **289** 419
[143] Nunner T and Kopp T private communication
[144] Grant J B and McMahan A K 1992 *Phys. Rev.* B **46** 8440
[145] Martin R L and Hay P J 1993 *J. Chem. Phys.* **98** 8680
[146] Eskes H, Tjeng L H and Sawatzky G A 1990 *Phys. Rev.* B **41** 288
[147] de Graaf C 1998 *PhD Thesis* University of Groningen
[148] Geserich H P, Scheiber G, Geerk J, Li H C, Linker G, Assmus W and Weber W 1988 *Europhys. Lett.* **6** 277
[149] Kuiper P, Guo J-H, Såthe C, Duda L-C, Nordgren J, Pothuizen J J M, de Groot F M F and Sawatzky G A 1998 *Phys. Rev. Lett.* **80** 5204
[150] Teske C L and Müller-Buschbaum H K 1969 *Z. Anorg. Allg. Chem.* **370** 134
[151] Kim T K, Rosner H, Drechsler S-L, Hu Z, Sekar C, Krabbes G, Málek J, Knupfer M, Fink J and Eschrig H 2003 *Phys. Rev.* B **67** 024516
[152] Yamashita Y and Ueda K 2000 *Phys. Rev. Lett.* **85** 4960
[153] Kotov V N, Zhitomirsky M E and Sushkov O P 2001 *Phys. Rev.* B **63** 064412
[154] Lemmens P, Choi K-Y, Kaul E E, Geibel C, Becker K, Brenig W, Valenti R, Gros C, Johnsson M, Millet P and Mila F 2001 *Phys. Rev. Lett.* **87** 227201
[155] Brenig W 2003 *Phys. Rev.* B **67** 064402